Aalto University

Enevoldsen, Georg H.; Pinto, Henry P.; Foster, Adam S.; Jensen, Mona C.R.; Kühnle, Angelika; Reichling, Michael; Hofer, Werner A.; Lauritsen, Jeppe V.; Besenbacher, Flemming

Detailed scanning probe microscopy tip models determined from simultaneous atom-resolved AFM and STM studies of the TiO$_2$ (110) surface

꒳

Detailed scanning probe microscopy tip models determined from simultaneous atom-resolved AFM and STM studies of the TiO$_2$(110) surface

Georg H. Enevoldsen,[1] Henry P. Pinto,[2] Adam S. Foster,[2] Mona C. R. Jensen,[1] Angelika Kühnle,[3] Michael Reichling,[3] Werner A. Hofer,[4] Jeppe V. Lauritsen,[1] and Flemming Besenbacher[1]

[1]*Interdisciplinary Nanoscience Center (iNANO) and Department of Physics and Astronomy,*
8000 Aarhus C, University of Aarhus, Denmark
[2]*Laboratory of Physics, Helsinki University of Technology, Finland*
[3]*Department of Physics, University of Osnabrück, Germany*
[4]*Surface Science Research Centre, The University of Liverpool, Liverpool, United Kingdom*

The atomic-scale contrast in noncontact atomic force microscopy (nc-AFM) images is determined by the geometry and exact atomic structure of the tip apex. However, the tip state is an experimentally unknown parameter, and the lack of insight into the tip apex often limits the possibilities of extracting precise quantitative and qualitative atomistic information on the surface under inspection. From an interplay between simultaneously recorded nc-AFM and scanning tunneling microscopy (STM) data, and atomistic STM simulations based on multiple scattering theory, we demonstrate how the state of the scanning probe microscopy (SPM) tip in the experiments may be determined. The analysis of a large number of experimental SPM images recorded with different tips reveals that no general correlation exists between the contrast observed in the nc-AFM and the tunneling current (I_t) images on TiO$_2$(110) surface. The exact state of the SPM tip must, therefore, be determined for each specific case, which is normally a very difficult endeavor. However, our analysis of the AFM contrast on TiO$_2$(110) surface allows us to considerably reduce the number of tips to be considered in a full simulation. By carefully evaluating the contrast of a handpicked library of SPM tips, we manage to determine a very accurate model of the SPM tip used in an experiment for the first time. It is envisioned that the approach presented here may eventually be used in future studies to screen for and select a SPM tip with a special functionalization prior to imaging an unknown sample, and in that way facilitate precise modeling and chemical identification of surface species.

PACS number(s): 68.35.bg, 68.37.Ps, 68.37.Ef, 68.47.Gh

I. INTRODUCTION

The most widely used scanning probe techniques are atomic force microscopy (AFM) and scanning tunneling microscopy (STM).[1–4] Both techniques are local scanning probe microscopy (SPM) techniques capable of imaging a surface with atomic resolution in real space, making it possible to study the atomic structure of a surface and pinpoint the location of individual point defects and adsorbates. The sensing principle in AFM and STM is, however, based on the measurement of quite different physical properties in a system consisting of a proximal probe and the surface. STM measures the tunneling of electrons through the tip-surface gap, and therefore, a STM image generally reflects a map of the tunneling probability often determined by a rather complex convolution of the geometric and electronic structures of the surface. AFM operated in the noncontact mode (nc-AFM) measures the local forces arising from the formation and breaking of chemical bonds between the surface atoms and the outermost tip-apex atoms while the tip is oscillated at a short distance above the surface atoms. The magnitude of the forces giving rise to atom-resolved nc-AFM imaging depends on the affinity of the tip-apex atoms to interact with the specific surface atoms. The atomic-scale contrast in AFM images may therefore be regarded as a convolution of the geometric properties of the surface and a "chemical" contribution that is tip dependent. Previous experimental and theoretical studies have attempted to reveal whether a universal

proportionality may exist between tunneling currents and forces.[5–7] However, a definitive conclusion has been hampered by the difficulties in achieving accurate simulations of experimental tunneling currents and forces since no, or at best, very little knowledge is generally available regarding the atomic-scale structure of the imaging tip apex. Nevertheless, recent results have demonstrated the great potential of simultaneous AFM/STM imaging.[8,9]

In the present study we overcome the problem associated with the lack of information about the imaging tip by analyzing a large set of simultaneously recorded atom-resolved topographic nc-AFM and tunneling current (I_t) images of the TiO$_2$(110) surface recorded with a number of different tip terminations. We make use of the fact that rather detailed knowledge on the nature of the tip apex is already available from previous nc-AFM studies and simulations of this surface.[10,11] Using these previous results as a starting point, we demonstrate that the complementary information provided by combining atom-resolved STM and AFM experiments greatly narrows the set of possible tip models needed to achieve good correspondence between experiments and image simulations. Hence, it provides a general route to unambiguous interpretation via simulations using realistic tip models. The results reveal that the contrast in both nc-AFM and STM images of the TiO$_2$ surface is highly dependent on the detailed atomic configuration of the tip apex, and no simple tip-independent proportionality can generally be expected between the recorded tunneling current and tip-

045416-1

surface forces. Furthermore, our results demonstrate the important finding that STM image simulations of the $TiO_2(110)$ surface, using the Tersoff-Hamann approach,[12,13] may lead to incorrect conclusions for some of the tips encountered in experiments.

II. METHODS

A. Experiment

Experiments were carried out at room temperature on a clean $TiO_2(110)$ single-crystal surface exposing the regular (1×1) termination [Figs. 1(a)–1(c)].[14] The surface was prepared prior to each experiment using ion bombardment, followed by annealing at ~950 K. The experimental setup, the operation of the nc-AFM, and the parameters for the $TiO_2(110)$ surface preparation have been described in detail elsewhere.[10] We used Si cantilevers (Nanosensors type NCH, $f_0 \sim 300$ kHz), which were initially treated with a light Ar^+ ion bombardment required to remove the native silicon oxide layer and render the tips conducting. The potential difference between tip and surface, U_{bias}, was monitored regularly and adjusted to minimize the electrostatic forces arising from the contact potential difference (CPD).[1,15] We found that the CPD changed significantly from 2–3 V for a pristine tip to 0.5–1.0 V for a tip cleaned by Ar^+ ion bombardment.

All images were recorded in the topographic nc-AFM mode (Z channel) where the tip traces the surface on contours of a predetermined constant frequency shift. The tunneling current (I_t channel) was recorded simultaneously as an additional passive signal and stored in a separate channel. When the I_t is recorded during nc-AFM experiments in this manner, it is important to note that the measured current signal is modulated in two ways: (i) by the oscillation of the cantilever in and out of tunneling, and (ii) by the motion of the tip apex determined by the Δf feedback setting.

The preamplifier for the tunneling current of our setup has a much lower bandwidth (10 kHz) than the oscillation frequency of the tip (typically 250–300 kHz) and the measured I_t is averaged over many oscillation cycles. In a large amplitude limit ($\kappa_t \times A_{p-p} \gg 1$) and neglecting relaxation effects, the measured averaged tunneling current ($I_{t,ave}$) is related to the maximum tunneling current at the lower turning point of the oscillation ($I_{t,max}$) through the expression[2]

$$I_{t,ave} = \frac{I_{t,max}}{\sqrt{2\pi\kappa_t A_{p-p}}}, \quad (1)$$

where κ_t and A_{p-p} are the tunneling current decay constant and the peak-to-peak oscillation amplitude.

The second modulation effect is more subtle and arises since the contours of constant Δf in nc-AFM topography images do not necessarily correspond to the actual geometric surface structure, as demonstrated in Ref 10. Due to the strong exponential distance dependence, the recorded I_t will therefore be strongly influenced by the actual motion of the tip perpendicular to the surface and one needs to take this into account when interpreting simultaneously recorded images. The recorded I_t images should, therefore, not be confused with regular constant-current STM images. However,
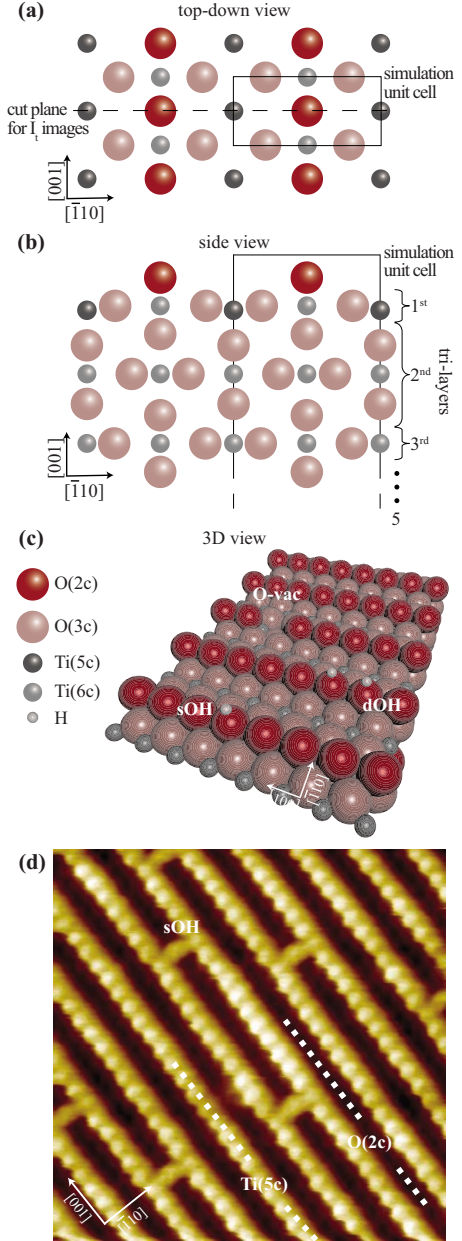

FIG. 1. (Color online) [(a)–(c)] Ball models of the $TiO_2(110)$ surface in side, top down, and 3D view, respectively. (a) and (b) are stoichiometric models whereas (c) has three surface defects: O-vac, sOH, and dOH. In (a) and (b), the unit cell used for simulations is indicated. (d) STM image of the $TiO_2(110)$ surface. The bright atomically resolved rows are identified as Ti(5c) rows and the bright protrusions in between the bright rows are identified as sOH groups. Image parameters (IP): Size=8×8 nm^2, U_{bias}=1.31 V, and I_t =0.75 nA.

they still provide information on the tunneling probabilities and hence the expected contrast in STM images. The possibility of a strong coupling between the oscillation motion of the tip and I_t could, in principle, be avoided by simultaneously recording both frequency shift and tunneling current images in the constant height mode of operation, where the tip traces the surface at a fixed distance. In fact, it has recently been demonstrated how a combination of scanning

with and without the feedback loop activated helped distinguish "real" image contrast from feedback loop crosstalk.[9] From recording numerous images, it is, however, our experience that constant height imaging is somewhat unstable on the rather corrugated $TiO_2(110)$ surface to sustain stable atomic resolution for a longer period.

B. Theory

1. System setup

The calculations of TiO_2 were performed using the plane-wave basis Vienna *ab-initio* simulation package (VASP),[16,17] implementing the generalized gradient approximation (GGA) by Perdew, Burke, and Ernzerhof (PBE).[18] Core electrons are described by projected augmented wave (PAW) potentials,[19] where the potential for the titanium atom was generated in the electron configuration $[Ne]3s^23p^64s^23d^2$, oxygen in $[1s^2]2s^22p^4$, hydrogen in $1s^1$, tungsten in $[Xe,4f^{14}]5p^65d^46s^2$, and silicon in $[Ne]3s^23p^2$ (square brackets denote the core electron configurations). Using a kinetic cut-off energy of 450 eV and a Γ centered $5 \times 5 \times 8$ k-point mesh (30 k points within the Brillouin zone of the corresponding primitive cell), we converge the total energy to <1 meV/f.u. (f.u.=formula unit TiO_2). The ionic optimizations were performed until all the forces were <0.01 eV/Å. The computed lattice parameters are $a=b$ =4.654 Å, c=2.973 Å, and u=0.305. Considering the well-known overestimation of bond lengths within GGA approximation, these values are in good agreement with the experimental ones: a_{Expt}=4.5936 Å, c_{Expt}=2.9587 Å, and u_{Expt} =0.3048.[14]

The properties of the $TiO_2(110)$ surface were modeled with five trilayers (O-TiO_2-O) along the Z direction and 15 Å vacuum thickness between slabs. Previous studies have shown that bond lengths in $TiO_2(110)$ are properly described by slabs with at least five trilayers (Ref. 20) although only slabs with more than 11 trilayers should achieve convergent surface energy and absolute ionic positions.[20] Using dipolar corrections and the same criteria as in the bulk for cut-off energy (450 eV), relaxation forces (<0.01 eV/Å), and k-point sampling density including Γ point, i.e., $8 \times 4 \times 1$ (15 k points within the Brillouin zone of the corresponding primitive cell), we relaxed the surface that is freezing the lowest two trilayers. The resulting structure is practically the same as in Ref. 21 and is in good agreement with recent high-resolution low-energy electron-diffraction measurements (LEED-IV).[22]

2. Calculating the current

The corrugation height is the most important feature of STM in constant-current mode for a given bias voltage. There are several methods and approximations to estimate the tunneling current (cf. to Ref. 23). The most simple model—and widely used—is the so-called Tersoff-Hamann (TH) approach.[12,13] Within this model, the STM current is proportional to the surface local-density of states (LDOS) at the position of the tip apex. In general this approximation provides important insight into surface topography but it has

limitations as it does not include the influence of the tip. One of the most sophisticated methods to model STM is the multiple electron scattering with a Green's-function formalism implemented in the BSKAN code.[24] This code uses the real-space single-electron wave functions of tip and surface (computed with VASP separately) and calculates the tunneling currents through a vacuum barrier. Within this barrier, the interaction between electrons is negligible; for typical tunneling conditions of ~1 nA, the time scale of processes is about 10^{-10} s—two or three orders of magnitude longer than the typical time scale of lattice relaxations.[25] With this in mind the STM can be simplified to the study of tunneling current between two leads (in thermal equilibrium) separated by a vacuum barrier. The applied bias potential modifies the chemical potential of surface (μ_S) and tip (μ_T), thus the tunneling current can be expressed through the Landauer-Bütticker formula,[26]

$$I(V) = \frac{2e}{h} \int_{\mu_T-eV}^{\mu_S-eV} dE[f(\mu_S, E) - f(\mu_T, E)]\text{Tr}[\Gamma_T(E)G^R(E)\Gamma_S(E)G^A(E)], \quad (2)$$

where $f(\mu_S, E)$ is the Fermi distribution, $\Gamma_{T(S)}$ is the coupling to the tip (surface), and $G^{R(A)}$ is the retarded (advanced) Green function of the barrier. Evaluating $I(V)$ in real space and doing calculations,[24] one can show that the tunneling current in the zero-order (first-order) approximation, including the effect of the bias voltage, is given by

$$I(V)_{0\text{-ord.}(1^{st}\text{-ord.})} = \frac{4\pi e}{\hbar} \sum_{ik} \left[f\left(\mu_S, E_k - \frac{eV}{2}\right) - f\left(\mu_T, E_i - \frac{eV}{2}\right) \right] \times \left| \left(-\frac{\hbar^2}{2m} - (+)\frac{eV}{k_i^2 - k_k^2}\right) M_{ik} \right|^2 \delta(E_i - E_k + eV), \quad (3)$$

where $E_i(k)$ are the eigenvalues of the tip (surface) wave functions and M_{ik} is called the tunneling matrix elements,

$$M_{ik} = \int_S dS[\chi_i^*(r)\nabla\psi_k(r) - \psi_k(r)\nabla\chi_i^*(r)] \quad (4)$$

where χ_i (ψ_i) are the Kohn-Sham wave functions of the tip (surface) in the vacuum region. Notice in Eq. (3) the quadratic dependence of the tunneling current with the bias voltage applied; this effect is observed in experiments.[27]

3. Simulated images

A library of ten chemically and structurally different tips was constructed, consisting of: (i) one tungsten (W) tip to be used for comparison with standard STM experiments, and (ii) the additional nine structurally and chemically different tips were all constructed to resemble real experimental tips likely to exist when scanning a TiO_2 surface using nc-AFM tips. These additional tips include clean silicon tips and silicon-based tips terminated with Ti_xO_y nanoclusters of dif-
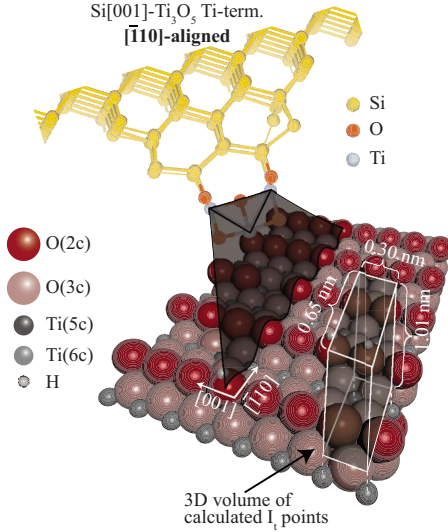
FIG. 2. (Color online) Ball models of one of the ten different tips and the TiO$_2$(110) surface. The plane defined by the three Ti atoms in the terminating Ti$_3$O$_5$ cluster of the tip model intersects the surface along the $[\bar{1}10]$ direction, as indicated by the gray plane, hence the tip labeling "$[\bar{1}10]$ aligned." Also indicated is the 3D volume of calculated I_t points (gray box with white edges) located above a stoichiometric surface unit cell [see Fig. 1(a)]. The size of the box is $0.30 \times 0.65 \times 1.01$ nm^3, as indicated, and contains 18 $\times 41 \times 95$ calculated I_t points.

ferent orientations and terminations. The orientation vectors assigned to each tip are defined such that the vector next to the bulk tip material, i.e., W(110) and Si(001), shows the crystallographic direction of the tip pointing toward the surface plane. The alignment vectors shown for the Ti$_x$O$_y$ clusters indicate the surface crystallographic direction parallel to the plane expanded by the three Ti atoms in the tip-terminating cluster, as shown in Fig. 2. For the Si-dimer tips, the alignment vector indicates the surface crystallographic direction of the terminating Si-Si bond. In the following, the calculated tunnel current (I_t) values are presented in two ways: Direct cut images, and space- and time-averaged images.

Direct cut images. The theoretically calculated three-dimensional (3D) volumes of I_t values (see Fig. 2) are presented as direct cuts in the $[110] \times [1\bar{1}0]$ plane at exactly the position of the O(2c) and Ti(5c) atoms [see Fig. 1(a)] with added constant I_t contours. This way of displaying the calculated I_t values provides a two-dimensional (2D) cross-section map illustrating the corrugation across the O(2c) and Ti(5c) atoms in a constant-current STM experiment.

Space- and time-averaged images. The theoretically calculated 3D volumes of I_t values were averaged along the [001] direction over the entire surface unit cell, reducing the initial 3D data volume to a 2D image lying in the [110] $\times [1\bar{1}0]$ plane representing an averaged I_t map across the Ti(5c) and O(2c) rows. Furthermore, to enable a direct comparison between the simultaneous Z and I_t experiments, and the theoretical calculations, the unit-cell averaged I_t maps were time averaged over an oscillation cycle of the AFM tip with an oscillation amplitude corresponding to the experi-

mental one. The oscillation amplitudes used for the experiments presented here were much larger than the size of the calculated 3D volume of I_t values in the [110] direction, i.e., $\gg 1.01$ nm. The I_t values beyond 1.01 nm in the [110] direction needed for the averaging were all assigned to zero. The oscillation averaging transforms the original calculated I_t maps into I_t maps representing images for an oscillating tip with each point in the map corresponding to the lower turning point (closest approach) of the oscillation. These space- and time-averaged calculated STM images are referred to as averaged images in the following sections.

III. RESULTS and DISCUSSION

A. Experiment results

Figure 1(d) depicts a typical atom-resolved constant-current STM image of the TiO$_2$(110) surface recorded with a W tip at room temperature. In the literature there is general agreement that for images recorded with a W tip, the parallel bright stripes running in the [001] direction should reflect the fivefold coordinated titanium atoms [Ti(5c)].[21,28–30] Between the Ti(5c) rows, twofold coordinated bridging oxygen atoms [O(2c)] are imaged as dark rows even though they geometrically protrude approximately 0.15 nm further from the surface.[20] In the following we refer to the stoichiometric surface sites [O(2c) or Ti(5c)] giving rise to largest tunneling currents as the primary tunneling sites (PTS). The somewhat counterintuitive appearance of the TiO$_2$(110) surface in STM can be traced back to a higher tunneling probability at the Ti(5c) surface sites, compared to the O(2c) for normal STM tip-surface distances. A simulation performed by the standard TH methods displaying the local-density of states at the Fermi level thus also associates the highest contrast to the Ti(5c) rows independent of the actual tip termination.[29,30] In sharp contrast to this observation, we have recently revealed from a detailed analysis of atom-resolved nc-AFM images of the TiO$_2$(110) surface presented in Refs. 10 and 11 that the contrast in nc-AFM images (i.e., which surface species produce bright and dark contrast in images) is highly dependent on the atomic-scale nature of the AFM tip apex. The contrast in nc-AFM is generated by the detection of small variations in the tip-surface force acting on an oscillating tip scanning the surface at a subnanometer distance. Tip-surface forces include both long-range van der Waals forces and short-range chemical forces emanating from the outermost tip apex with the latter being responsible for atomic-scale contrast formation. In atom-resolved nc-AFM images of TiO$_2$, it was observed that either the sublattice [see Fig. 1(a)–1(c)] of Ti atoms (formally charged as Ti^{4+}) or O atoms (charged as O^{2-}) appeared with a bright contrast in nc-AFM images for different tip terminations, corresponding to a maximum interaction of the AFM tip over either of these sites.[10,11] The variation of the atomic AFM contrast was successfully explained by considering the polarity of the specific type of tip apex. The electrostatic forces arising between the surface ionic sublattice and the polarized or charged tip-apex atom were seen to dominate the nc-AFM images contrast formation, leaving the atomic-scale geometric structure of the surface as a secondary effect. Since a negatively terminated tip

(e.g., O terminated) interacts strongly with the positive Ti^{4+} sublattice, such a tip will image these sites with a bright contrast and vice versa for a positively terminated tip. A neutral tip termination (e.g., pure Si tip) was also identified (Ref. 10) and, with the electrostatic interaction between the tip and the surface being significantly reduced, the resulting contrast thus reflects the atomic-scale geometry of the surface. The different tips were generated by random contact with the surface or adsorption onto the tip apex, and such tip changes are common to most SPM experiments. In the following we will show how the qualitative and quantitative contrasts in atom-resolved tunneling current (I_t) images also varies with the type of tip termination. The complementary information in nc-AFM topographic images (Z) and the tunneling images (I_t) is then used in Sec. III B to construct accurate tip models corresponding to each contrast mode. It should be noted that a number of defects and adsorbates associated with oxygen vacancies (O-vac), single hydroxyls (sOH), and double hydroxyls (dOH) exist on the $TiO_2(110)$ surface prepared under UHV conditions.[31–33] In Fig. 1(c) a schematic 3D ball model of the $TiO_2(110)$ surface is shown, illustrating the geometry of the surface and the structure of O-vac, sOH, and dOH defects. All of these defect species are located on the O(2c) rows, and can therefore be used as markers to indicate the position of the O(2c) and Ti(5c) sublattices.[10,11]

1. Protrusion mode imaging

Figures 3(a) and 4(a) depict nc-AFM topography images (Z) with corresponding simultaneously recorded tunneling current images (I_t) shown in Figs. 3(b) and 4(b), respectively. As outlined in Refs. 10 and 11, the nongeometric appearance of the nc-AFM images in Figs. 3(a) and 4(a) can be understood by considering the AFM tip-apex polarity. The electrostatic forces arising between the surface ionic sublattice and the polarized or charged tip-apex atom dominate the nc-AFM image contrast formation, in this case, where the positively charged Ti(5c) (formally Ti^{4+}) rows appear as bright and the negatively charged O(2c) (formally O^{2-}) rows appear as dark. In addition to this, O-vac, sOH, and dOH species are visible in Fig. 3(a), and sOH are visible in Fig. 4(a), all of which are imaged as protrusions of varying brightness and lateral size located on the dark O(2c) rows. This type of nc-AFM image contrast is referred to as the *protrusion* mode due to the image contrast of the hydroxyl groups, which are imaged in this way since they are slightly positive relative to the O^{2-} rows.[10,11] From a comparison of the simultaneously recorded Z and I_t images in Figs. 3(a) and 3(b), it is evident that the image contrast is reversed, i.e., the O(2c) rows are imaged bright and the Ti(5c) rows are imaged dark, and the O-vac, sOH, and dOH are imaged as dark depressions on the bright atomically resolved O(2c) rows in the I_t image. In the following we refer to this as the "out-of-phase" imaging mode. Figure 4(a) was also recorded with a negatively terminated tip, i.e., in the protrusion mode. However, the corresponding I_t image contrast in Fig. 4(b) is not reversed in this case with the I_t image also resolving the Ti(5c) rows bright, the O(2c) rows dark, and the sOH imaged as bright
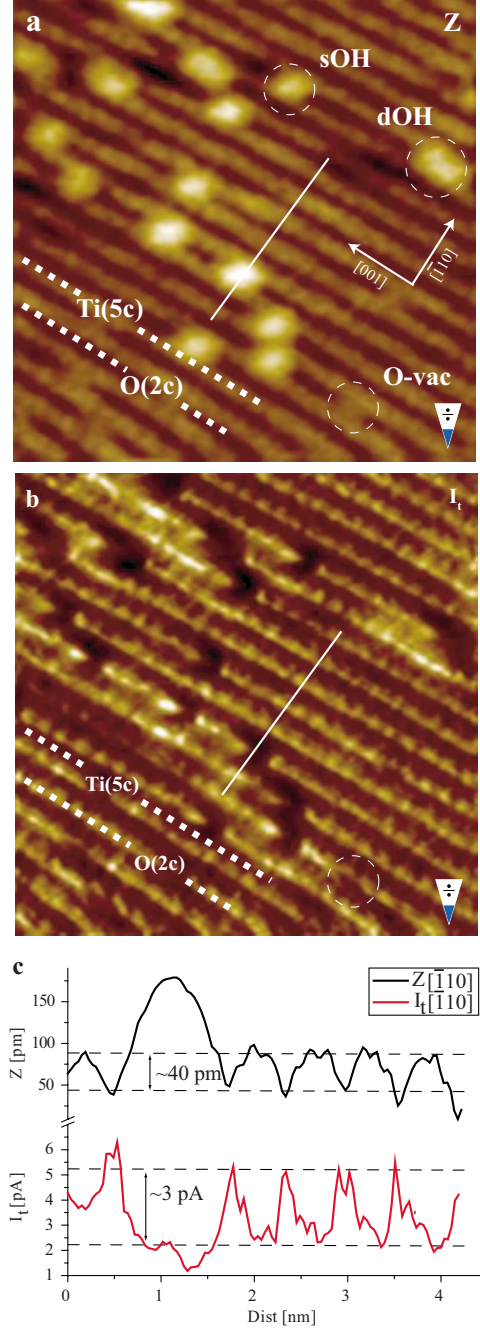

FIG. 3. (Color online) (a) High-resolution nc-AFM protrusion mode topography images (Z) of the $TiO_2(110)$ surface obtained with a negatively terminated tip. Imaging parameters (IP): Size $=10\times10$ nm^2, $\Delta f=-45$ Hz, $U_{bias}=0.93$ V, and $A_{p-p}\sim26$ nm. (b) Simultaneous recorded tunneling current images (I_t). (c) Twin cross-section pairs taken along the white solid lines in (a) and (b). sOH, dOH, and O-vac are visible, labeled, and indicated by white dashed circles in (a).

features in between the bright Ti(5c) rows. We refer to this as the "in-phase" imaging mode.

The out-of-phase imaging mode of Figs. 3(a) and 3(b) indicates that the vertical motion of the AFM tip, as it traces across the surface on a contour of constant frequency shift, seems to dominate the I_t image contrast through the expo-
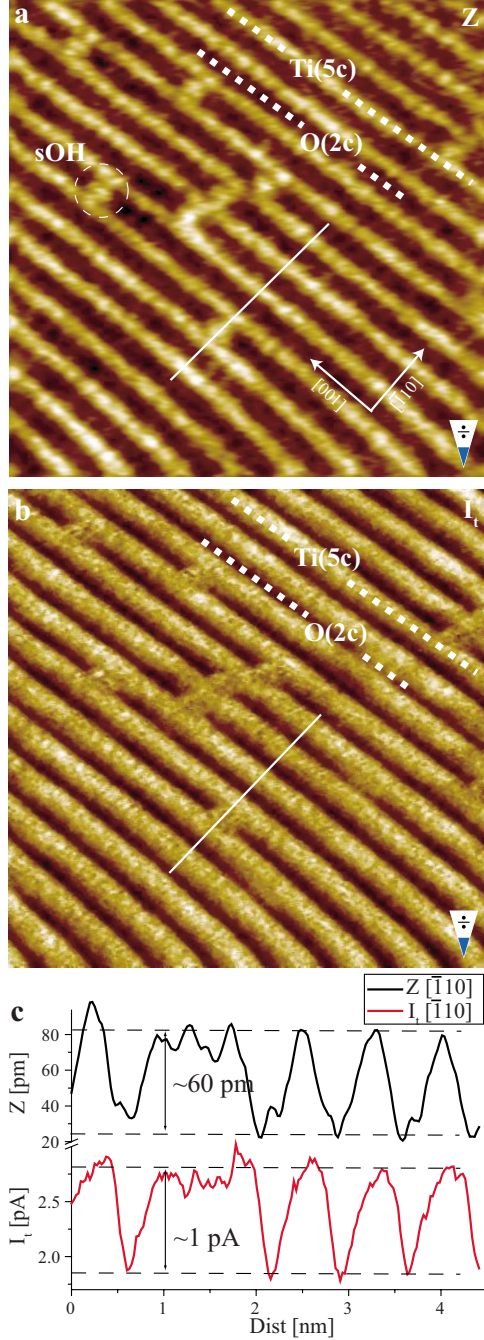
FIG. 4. (Color online) (a) High-resolution nc-AFM protrusion mode topography images (Z) of the $TiO_2(110)$ surface obtained with a negatively terminated tip. IP: Size=10×10 nm^2, $\Delta f =$ -46.9 Hz, $U_{bias}=0.97$ V, and $A_{p-p} \sim 26$ nm. (b) Simultaneous recorded tunneling current images (I_t). (c) Twin cross-section pairs taken along the white solid lines in (a) and (b). Only sOH are visible, one is indicated in (a).

nential distance dependence of I_t. Published theoretical calculations based on the TH approach[12,13] consistently predict the Ti(5c) rows as the PTS.[29,30] However, it is clear from this analysis that here the O(2c) rows were imaged bright in the I_t images, seemingly because here the tip could be brought in closer proximity to the surface.

The in-phase imaging mode of Figs. 4(a) and 4(b) allows for an unambiguous identification of the PTS as being the Ti(5c) rows, in agreement with the simple TH approach. Here, the Ti(5c) rows were imaged as bright in the I_t image even though the tip here retracted from the surface, which indicates that the tunneling probability over the Ti(5c) sites must be significantly larger than those over the O(2c) sites in order to surmount the increased tip-surface imaging distance. The graphs in Figs. 3(c) and 4(c) show parallel cross-section pairs taken along identical paths (twin cross sections) in Figs. 3(a) and 3(b), and Figs. 4(a) and 4(b), respectively, as indicated by the white solid lines. The Z corrugation of the nc-AFM images shown in Figs. 3(a) and 4(a) is measured to be ~ 40 pm and ~ 60 pm, respectively, while the I_t corrugation of Figs. 3(b) and 4(b) is measured to be ~ 3 pA and ~ 1 pA, (of opposite sign) respectively. The I_t cross sections of the graphs in Figs. 3(c) and 4(c) also reveal that the absolute measured I_t values are markedly different with a maximum value of ~ 2.75 pA for the image in Fig. 3(b), compared to a significantly larger maximum value of ~ 5 pA for the image in Fig. 4(b). It is interesting to note that the corrugation in the Z images across the Ti(5c) and O(2c) rows in the [$\bar{1}10$] direction, shown in the graphs in Figs. 3(c) and 4(c), is larger for the image in Fig. 4(a) as compared to the corrugation in Fig. 3(a), and that also the signature of the sOH differs. We attribute this difference to the fact that the nc-AFM image in Fig. 4(a) was recorded closer to the surface compared to Fig. 3(a), as presented in our previous work.[10] The absolute measured I_t values were, however, larger in Fig. 3(a) as compared to Fig. 4(b), which indicates that the tunneling properties must indeed be strongly influenced by the detailed chemical and structural composition, and the resulting electronic structure of the probing tip apex.

2. Neutral mode imaging

The nc-AFM topography images (Z), shown in Figs. 5(a) and 6(a), have been recorded in a mode that depicts more closely the geometric structure of the surface, which we will thus subsequently refer to as the *neutral* mode.[10] In this mode, the bright rows represent the O(2c) rows and the additional bright protrusions, imaged on top of the bright O(2c) rows, are assigned to sOH groups. Due to the very good agreement between the nc-AFM image contrast and the geometric structure of the $TiO_2(110)$ surface [Figs. 1(a)–1(c)], the tip-apex polarity is consequently interpreted as being neutral since the polarity of the different surface ions no longer dominates the interaction with the AFM tip and thereby the image contrast. A possible tip model might be a pure silicon tip, as also argued in Ref. 10. The tunneling current (I_t) image corresponding to Fig. 5(a) is shown in Fig. 5(b) and it is seen that these two images have been recorded in the out-of-phase mode, with the bright rows in the I_t image consequently being identified as the Ti(5c) rows with the individual Ti atoms clearly resolved. The sOH that appear bright in the Z image are conversely imaged as very shallow dark pits on the dark O(2c) rows in the I_t image. In contrast, the corresponding Z and I_t images in Figs. 6(a) and 6(b) have been recorded in phase, both resolving the O(2c) rows bright with bright sOH on top. As in the case of Figs. 4(a) and 4(b),
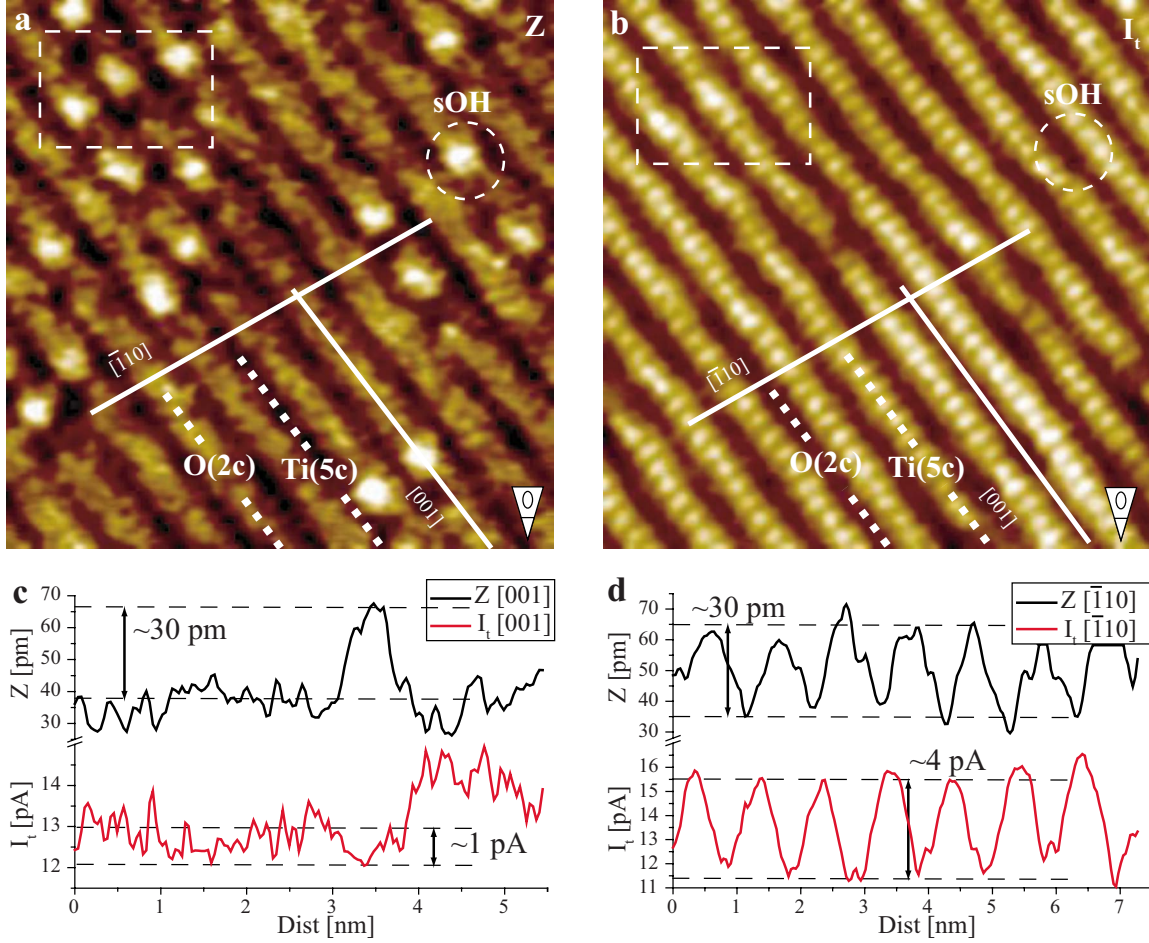
FIG. 5. (Color online) (a) High-resolution nc-AFM topography images (Z) of the $TiO_2(110)$ surface obtained in the "neutral" mode with an electrostatically neutral tip termination. IP: Size=10×10 nm^2, $\Delta f = -53$ Hz, $U_{bias} = 0.97$ V, and $A_{p-p} = \sim 26$ nm. (b) Simultaneously recorded tunneling current images (I_t). One sOH is labeled and marked by white dashed circles. [(c) and (d)] Twin cross sections of the Z and I_t images indicated by the white solid lines. The white dashed box in (a) and (b) indicates sOH signature located also on the Ti(5c) rows, most likely due to a double-tip phenomenon.

this allows us to unambiguously identify the O(2c) rows as the PTS. Twin cross sections, taken along the [001] direction directly on top of the O(2c) rows, as indicated by the white solid lines, are shown in the graphs in Figs. 5(c) and 6(c). In the Z images, the height of the sOH relative to the O(2c) row is almost identical, measuring ~ 28 pm and ~ 30 pm, respectively. However, due to the in-phase and out-of-phase imaging modes, the sOH signatures in the corresponding I_t images are quite different, and are measured to be ~ -1 pA and ~ 1 pA, respectively.

The unambiguous identification of the O(2c) rows as the PTS for the images in Fig. 6 already contradicts the general identification of the Ti(5c) as the PTS based on TH simulations. There have been reports of changes in the PTS on the $TiO_2(110)$ surface with the PTS switching from the Ti(5c) to the O(2c) rows,[34] which are proposed to occur at very small imaging distances. This effect might explain the evidence of the O(2c) rows acting as the PTS in Figs. 6(a) and 6(b). However, the very similar Z image contrast of Figs. 5(a) and 6(a), and the identical frequency shift set point indicate that these two images were recorded at approximately the same imaging distances. Also, from Eq. (1) using a typical value

for $\kappa_t \sim 10$ nm^{-1}, the maximum I_t value occurring at the closest approach is estimated to be ~ 400 pA, which is only considered as a moderate I_t value and not characteristic of very small tip-surface distances. Combining these two observations, the shift in PTS is most likely not caused by very close imaging distances and must rather be a tip-related effect.

For the images in Figs. 5 and 6 we again observe that although tip polarity, applied bias voltage, and Z corrugation are identical for the Z images, the corresponding simultaneously recorded I_t images can be both in phase and out of phase with a noticeable difference in the absolute value of the I_t recorded. We thus conclude that the tunneling properties of the tip-surface system must be influenced by the chemical and/or the nanoscale structure of the tip apex.

3. Hole mode imaging

In Fig. 7(a) it shows a nc-AFM topography image (Z) recorded with a cation terminating the tip apex. The positively terminated tip in this case causes the O(2c) rows to be imaged as bright and the Ti(5c) rows as dark, and the dark holes located on the bright O(2c) rows are identified as sOH
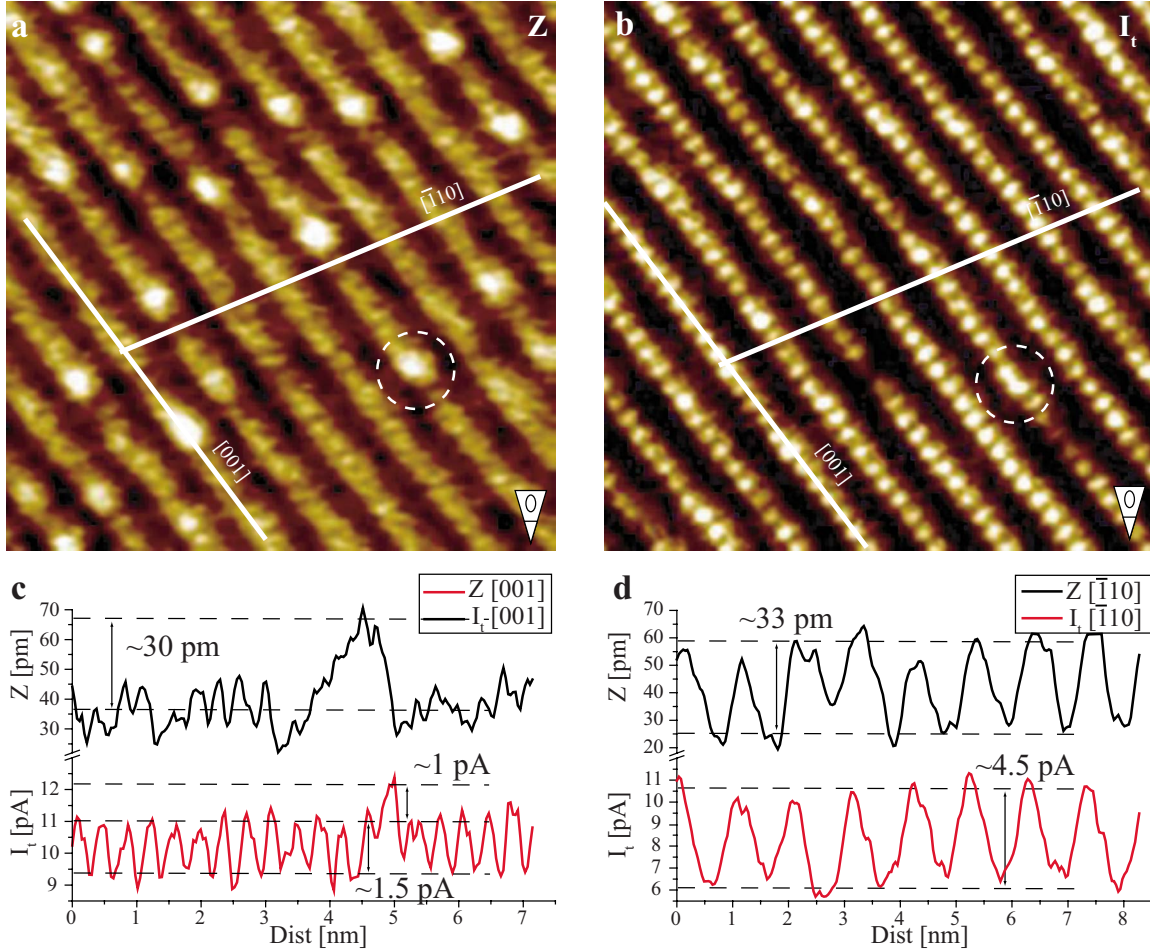
FIG. 6. (Color online) (a) High-resolution nc-AFM topography images (Z) of the $TiO_2(110)$ surface obtained with a "neutral" tip termination. IP: Size$=10\times10$ nm^2, $\Delta f=-53$ Hz, $U_{\mathrm{bias}}=0.97$ V, and $A_{p\text{-}p}=\sim26$ nm. (b) Simultaneously recorded tunneling current images (I_t). sOH are marked by white dashed circles. [(c) and (d)] Twin cross sections of the Z and I_t images indicated by the white solid lines.

and dOH (see Refs. 10 and 11). In the following, this type of Z image contrast is referred to as *hole* mode, reflecting the image signature of the hydroxyl groups, which now appears dark due to the fact that they are slightly less negative relative to the O^{2-} A rows. The corresponding tunneling current (I_t) image, shown in Fig. 7(b), is recorded in the out-of-phase mode, i.e., with the Ti(5c) rows imaged bright, the O(2c) rows imaged dark, and the sOH and dOH imaged as bright protrusions in between the bright Ti(5c) rows. Two sets of simultaneously recorded twin cross sections taken along the $[\bar{1}10]$ and $[001]$ directions are shown in the graphs in Figs. 7(c) and 7(d), respectively. In the graph in Fig. 7(c) the Z and I_t corrugations along the $[\bar{1}10]$ direction are measured to be ~25 pm and ~2 pA, respectively. Even though the I_t image contrast in Fig. 7(b) resembles the STM image contrast in Fig. 1(d), it is not straightforward to identify the Ti(5c) sites as the PTS since the images in Figs. 7(a) and 7(b) were recorded in the out-of-phase mode, and the I_t image contrast may therefore simply be the result of the tip Z motion across the surface (cross talk).

From the results of the Z image in Fig. 7(a) alone, it may be difficult to distinguish the sOH and dOH as they have very similar appearances. The twin cross sections shown in

Fig. 7(d), recorded along the $[001]$ direction, reveal that the depth of the sOH and dOH is almost identical, corresponding to ~60 pm and ~65 pm, respectively. In the I_t image in Fig. 7(b) the sOH and dOH are, however, easily distinguishable with the I_t peak values corresponding to ~5 pA and ~8.5 pA, respectively. This may be explained by considering both the exponential distance dependence of the electron-tunneling process amplifying the small difference in the depths of the sOH and dOH groups, and the fact that STM imaging shows an increased tunneling probability over the dOH site.[31] This serves as a nice example of how the simultaneous recording of nc-AFM topography and tunneling current signals complement each other, and how the combined information gained aids in the interpretation of the recorded images.

4. Summary of the experimental results

In the previous sections, the results for the three distinctively different nc-AFM contrast modes; protrusion, neutral, and hole modes were presented along with a variety of different types of I_t resolution. A detailed summary showing which combinations of nc-AFM topographic and tunneling current image contrast that were observed experimentally is
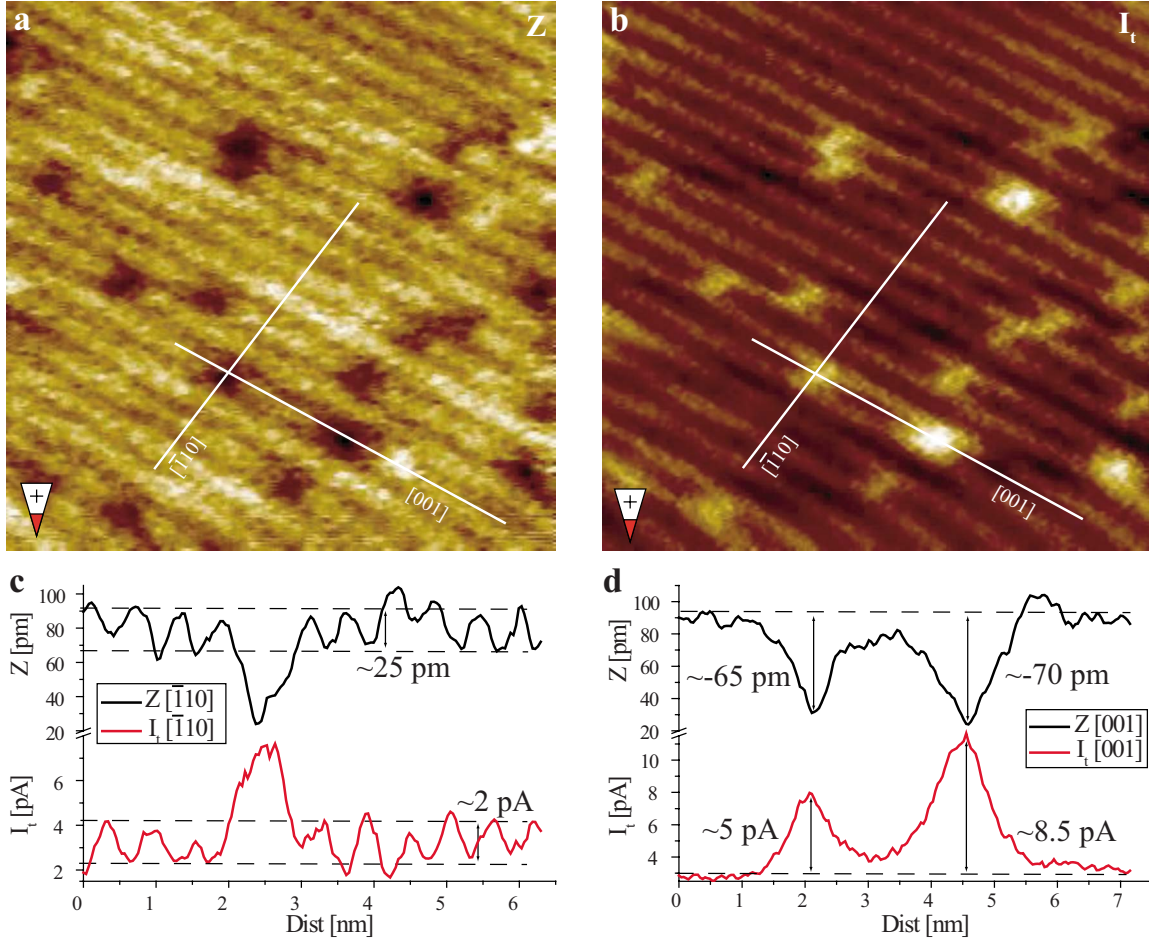
FIG. 7. (Color online) (a) High-resolution nc-AFM hole mode topography images (Z) of the $TiO_2(110)$ surface obtained with a positively terminated tip. IP: Size$=10\times10$ nm^2, $\Delta f=-45$ Hz, $U_{bias}=0.93$ V, and $A_{p-p}\sim28$ nm. (b) Simultaneously recorded tunneling current images (I_t). [(c) and (d)] Twin cross section pairs of the Z and I_t images indicated by the white solid lines. In (a) and (b), sOH and dOH are visible along the bright/dark O(2c) rows.

presented in Table I. As is evident from the results in Table I, almost any combination of contrast is observed and the observations underline the fact that detailed knowledge on the atomic-scale structure of tip apex is a prerequisite for determining the structure of a complex surface such as $TiO_2(110)$ (and species adsorbed thereon) without any independent complementary information. The only lacking contrast combination is the simultaneous recording of a hole mode nc-AFM image with the I_t image being in phase, also imaging the O(2c) rows bright. This lack, however, does not imply that this particular combination of image contrasts is unattainable; only that we have not yet observed it experimentally. Evidently, the detailed atomistic chemical, structural, and, hence, electronic structure of the scanning probe tip apex plays a key role in the electron-tunneling process generating the I_t image contrasts, as well as the forces determining the nc-AFM contrast. The wealth of contrast modes observed experimentally clearly suggest that many different generic types of tips may be formed, and in order to systematically investigate and understand how a specific contrast arises, we will in the following address each of the contrast modes and construct detailed atomistic tip-apex models that result in the observed contrast in both nc-AFM and I_t images.

B. Theory calculations

We have carried out theoretical calculations of I_t images of the stoichiometric $TiO_2(110)$ surface for ten chemically and structurally different tips. The library of tips includes one tungsten tip, two clean silicon tips, and seven silicon-based tips terminated with Ti_xO_y nanoclusters of different orientations and terminations (see Sec. II for details). The "contamination" of the clean silicon tips with Ti_xO_y material is highly likely to occur since the tip often comes in close contact (accidentally or deliberately) with the surface and thereby an exchange of material occurs.[10,11] Ball models of all tips along with both direct cuts of the calculated images and top-down images are included in the Appendix. Presented in Table II below is a summary of the theoretical I_t calculations, listing tip-apex polarity (determining the type of nc-AFM image contrast), and PTS (for distance >0.25 nm) for the individual tips modeled.

We have included a simulation of the $TiO_2(110)$ using a W tip in Fig. 8(a) in order to test the theoretical simulation against the large body of STM experiments obtained with W tips. In agreement with the results from numerous previous STM experiments[21,28,29] and the results from the STM image presented in Fig. 1(d), the I_t cross-section image shows high/

TABLE I. (Color online) Showing the different experimentally verified combinations of simultaneously recorded nc-AFM topographic and I_t image contrasts.

Resulting I_t image contrast	nc-AFM topographic resolution		
	Protrusion mode	Hole mode	Neutral mode
I_t out-of-phase	✓	✓	✓
I_t in-phase	✓	?	✓

bright contrast (larger I_t values) over the Ti(5c) sites at small to moderate constant I_t values. At very large constant I_t values, i.e., very small separation distances, the W tip actually results in bright contrast contours over the O(2c) atoms. This finding is in good agreement with a previously published theoretical calculation.[30] The corrugation of the constant I_t contours does, however, not seem to match quantitatively with what has been reported for constant-current STM experiments. In Fig. 8(b) is depicted a zoom-in of Fig. 8(a), showing the 300 pA constant I_t contour, which, as indicated, has a corrugation of ∼100 pm and is located ∼300 pm from the O(2c) surface atoms. These values disagree quantitatively with standard STM results on two accounts: First, a set point of I_t=300 pA is not a particularly large I_t set point value for constant-current STM imaging and thus one would assume that the tip would be probing the surface at considerably larger distances than the ∼300 pm indicated in Fig. 8(b). Second, the resulting constant I_t corrugation for the 300 pA contour is much larger compared to recently published STM results,[21] where a 30 pm corrugation over the Ti(5c) and O(2c) rows was reported for an I_t set point of 300 pA. If the initially calculated I_t values for the W[110] tip are scaled up by a factor of 200, the agreement is, however, almost perfect—as shown in Figs. 8(c) and 8(d). The zoom in on the resulting constant contour of I_t=300 pA [Fig. 8(d)] shows that not only has it moved further from the surface and is now located at a more reasonable 620 pm distance from the surface but also the resulting corrugation of ∼30 pm matches the reported corrugation in Ref. 21 almost perfectly. It is beyond the scope of the present study to account for these quantitative disagreements in detail but the origin of the discrepancy can be traced back to several sources. First, the BSKAN code[25,35] (see Sec. II) used for the I_t calculation does not allow the atoms in the tip and surface to relax prior to the evaluation of the I_t when the surface model consists of more than one type of atoms.[36] This effect may increase the measured I_t significantly. Second, the STM experiments are performed on a reduced TiO$_2$ crystal and states introduced in the band gap, e.g., by Ti bulk interstitials,[37] have been shown to increase the overall conductivity of the TiO$_2$ crystal.[38–40] The theoretical calculations are performed on a stoichiometric surface model and it is therefore to be expected that the theory should produce calculated I_t values that are too low. Finally, the silicon tips used in experiments were doped

to increase conductivity, whereas undoped silicon tips were used in theoretical simulations.

C. Identifying the imaging tip structure and chemical composition

From our previous extensive nc-AFM analyses of the TiO$_2$(110) surface,[10,11] we determined in Sec. III A the polarity of the imaging tip apex. However, there are many different ways in which we can construct, e.g., a positively terminated AFM tip. Using the combined information available from both the Z and the simultaneously recorded I_t images, it is possible to further reduce the number of possible tip model candidates, as tips producing the same type of nc-AFM image contrast (i.e., have the same tip-apex polarity) may yield entirely different I_t image contrast. From the "library" of tips used in our calculations, we can isolate and pick out a single tip that matches both the experimental Z and I_t image contrasts. This makes the selected tip model a highly likely candidate to represent the actual experimental tip and in the following it is referred to as the "primary tip candidate." To substantiate the choice of tip model further, a direct quantitative comparison between experiments and calculations is performed. The calculated I_t data for the tip model in question are converted to an averaged image, as described in Sec. II. The resulting images are subsequently compared with the experimentally measured I_t values in the following way: The experimentally measured Z cross sections in Figs. 3(c), 4(c), 5(d), and 6(d) are fitted with a periodic function (a sum of eight sines) to produce smooth periodic traces. If the experimental cross section included an sOH [Figs. 3(c), 4(c), and 7(c)], this part was excluded during the fitting process. These periodic function fitted (PFF) traces are then superimposed on the calculated averaged I_t cross-section maps and the corresponding I_t values are extracted. The initial averaging of the calculated I_t images is performed to mimic the oscillation of the tip, and to reduce the influence of experimental noise and measurement uncertainties associated with the exact position of experimentally measured cross sections. It should be noted that the superimposed PFF traces were shifted slightly by ∼±20° (or equivalently ∼±36 pm), depending on whether the corresponding nc-AFM image was recorded in the forward or backward fast-scanning direction. This shift compensates for the approximate delay of the Z-feedback loop relative to the surface topography, as estimated from a statistical analysis of simultaneously recorded Z and I_t images.[41] This slight shift of the Z cross section has a measurable effect on the extracted I_t values, and hence it is a nontrivial effect to include when performing a detailed qualitative and quantitative analysis of the recorded images. The resulting extracted calculated I_t values can then be used to make a direct comparison with the experimentally measured I_t cross sections, both qualitatively by comparing whether the Z and I_t signals are in phase or out of phase, and quantitatively by comparing the absolute I_t values.

1. Protrusion mode tip identification

Out of phase. For the recorded images in Figs. 3(a) and 3(b), we know from our previous results[11] that the tip must

TABLE II. (Color online) List of corresponding PTS as determined from theoretical calculations and tip-apex polarity. For tip 6 the tunneling probability is almost identical for the Ti(5c) and O(2c). Note that tips 6 and 10 are terminated by an OH group.

Tip #	1	2	3	4	5	6	7	8	9	10
PTS	Ti(5c)	Ti(5c)	O(2c)	O(2c)	O(2c)	"O(2c)"	O(2c)	O(2c)	O(2c)	O(2c)
Tip-apex polarity	0	÷	0	0	÷	+	÷	+	+	+

have a negatively charged tip-apex atom to generate the protrusion mode Z image contrast, where the Ti(5c) rows and hydroxyl groups are imaged as bright protrusions relative to the dark O(2c) rows. From the I_t image it is evident that the tip must either have the O(2c) rows as the PTS, or alternatively the Ti(5c) rows, with the requirement that in the latter case the tunneling probability over the Ti(5c) and O(2c) sites is relatively similar, as otherwise the Z corrugation would not be able to dominate the I_t image contrast. The negative termination criteria match the tip models for tips 2, 5, and 7 shown in the Appendix in Figs. 14(d), 15(a), and 15(c), respectively. However, since the experimental I_t corrugation [see Fig. 3(c)] is fairly high and has a spikelike structure, it is likely that the tip model should have the O(2c) rows as the PTS, excluding the tip 2 model. Since tip 7 produces very

low calculated I_t values, orders of magnitude smaller compared to tip 5, tip 5 is proposed as the primary tip candidate for the recorded images in Figs. 3(a) and 3(b). Tip 5 [also shown in Fig. 9(a)] is a Si-based tip terminated with a Ti_3O_5 nanocluster, oriented so that an O atom sits at the tip apex providing the required negative tip termination. To verify the selection of tip 5, a direct comparison is presented in Fig. 9. The calculated averaged I_t cross-section map with the PFF tip trace superimposed is depicted in Fig. 9(b) and the identical PFF tip trace along with the corresponding extracted I_t signal from Fig. 9(b) are shown in the graph in Fig. 9(d). On a qualitative level, the Z and I_t curves in Fig. 9(d) match excellently with the corresponding Z and I_t cross sections in Fig. 3(c) [also shown in Fig. 9(c)]. The Z and I_t signals are clearly out of phase, and also with the spikelike structure of
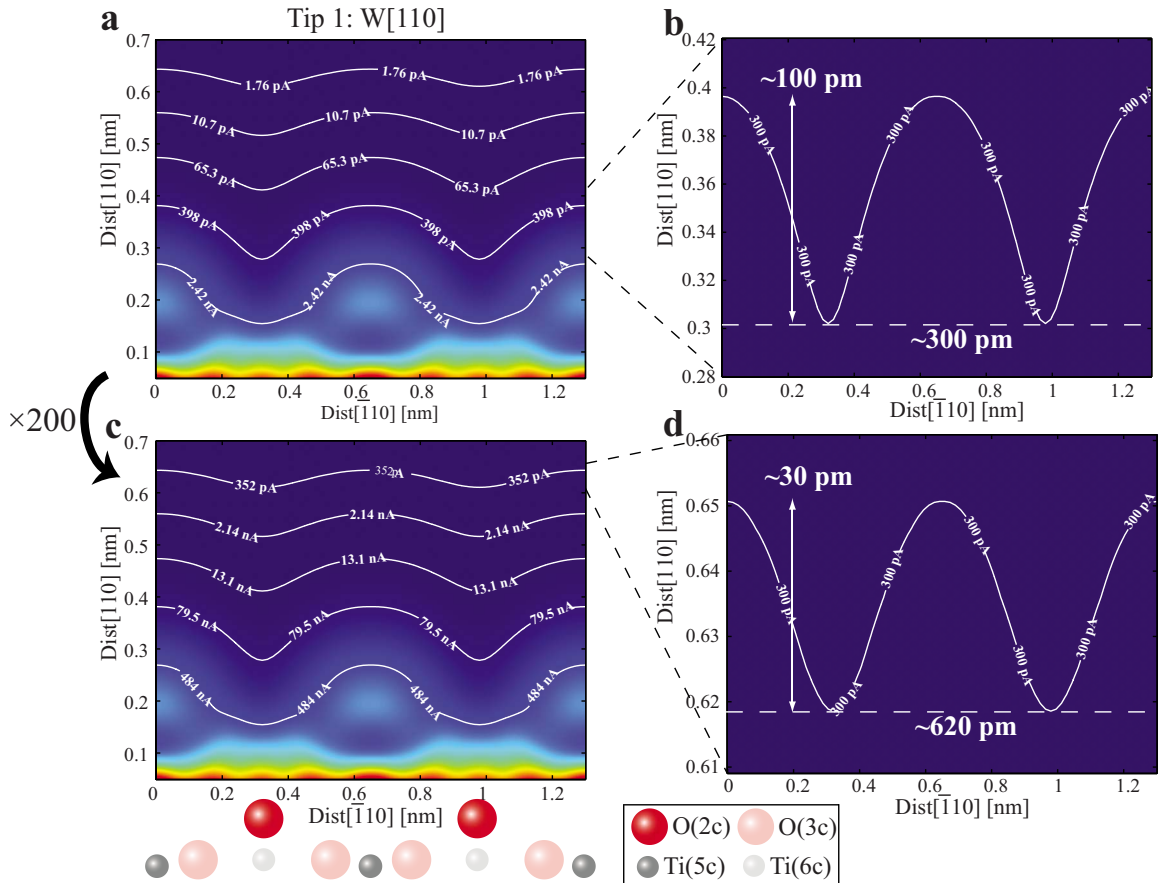

FIG. 8. (Color online) (a) Calculated I_t map for the W[110] tip (tip 1) taken across the Ti(5c) and O(2c) rows. (c) Same as (a), only scaled by a factor of 200. Below (c), a ball model indicates the positions of the different types of atoms in top-most surface layer. Both (a) and (c) show five logarithmically and equidistantly spaced constant I_t contours. [(b) and (d)] Zoom ins of (a) and (c), respectably, showing the position of the 300 pA constant I_t contour.
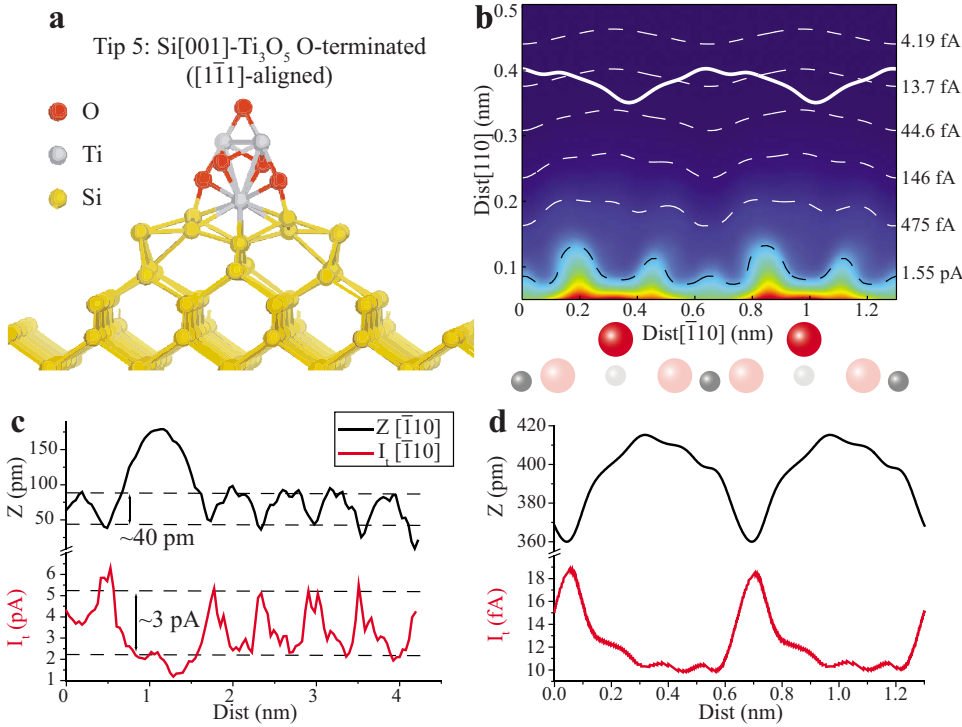
FIG. 9. (Color online) (a) Ball-and-stick model of tip 5. (b) Space- and time-averaged I_t images of the full 3D calculated volume corresponding to Fig. 15(a). Six contours of constant I_t value, logarithmically and equidistantly spaced between the maximum and minimum I_t value, are shown (five white dashed and one black dashed). Inserted (solid white) is the PFF trace of the experimental Z cross section in (c) (for ball-model color code, see Fig. 8). (c) The equivalent experimental cross section from Fig. 3(c). (d) The PFF trace along with the extracted corresponding I_t values from (b).

the I_t, the signal is reproduced. A comparison of the absolute measured and calculated I_t values, however, reveals a discrepancy since the experimental I_t values range from approximately 2–5 pA, whereas the calculated I_t values are lower by a factor of $\sim$200, ranging from approximately 10–20 fA. It should be noted that it is difficult to predict exactly how far above the surface the experimental Z trace should be evaluated and, obviously for smaller tip-surface distances, the resulting extracted I_t values will increase. However, even at very small distances, the calculated I_t values are still far from the experimental values, as is evident from the constant I_t contours depicted as dashed white and black curves in Fig. 9(b), and the error in the Z reference level is not likely to account for the differences alone. Also, from our previous results presented in Ref. 10, it is clear that the type of Z image contrast in Fig. 3(a) is not associated with small tip-surface imaging distances. The discrepancy of a factor of $\sim$200 matches the analysis of the W tip presented previously, supporting that the theoretically calculated I_t values underestimates the measured values. The error in the current associated with the uncertainty in the Z-reference level for the STM and AFM signals was recently discussed by Ternes *et al.* who demonstrated how a value for the Z reference point could be obtained as the point of tip-surface contact for a tuning fork AFM.[42] However, this method is not directly applicable to a cantilever-based AFM used here since it does not probe forces in the repulsive "contact" regime.

In phase. For the images presented in Figs. 4(a) and 4(b), there are, as previously mentioned, very strict criteria for selecting a tip model. The tip must be negatively terminated (protrusion mode) and it must have the Ti(5c) rows as PTS. This requirement matches perfectly and only with tip 2 shown in Fig. 10(a), and we identify this as the primary tip candidate. Tip 2 is a Si-based tip terminated by a Ti_3O_5

nanocluster, oriented such that an O atom sits at the tip apex. Tip 2 is very similar to tip 5 from the previous protrusion mode out-of-phase comparison. Only the structural arrangement of the Ti_3O_5 nanocluster is different, which leads to significantly different resulting I_t image contrasts, as is evident by comparing the calculated I_t images in Figs. 9(b) [Fig. 14(d)] and 10(b) [Fig. 15(a)]. For the direct comparison, the calculated averaged I_t cross-section map and graph of PFF tip trace, and resulting extracted calculated I_t signal are shown in Figs. 10(b) and 10(d), respectively. When compared with the experimentally measured Z and I_t cross sections in Fig. 4(c), also shown in Fig. 10(c), the graph in Fig. 10(d) is again in qualitative agreement. The Z and I_t curves are now in phase with the Z curve shifted slightly to the left relative to the I_t curve. A detailed analysis of the experimental cross sections in Fig. 10(c) shows they also are slightly shifted with the Z curve shifted slightly to the left relative to the I_t curve, implying that the qualitative agreement is very good. This slight shift of the Z and I_t curves is a result of the previously mentioned delay imposed by the finite speed of the Z feedback loop. A quantitative comparison of the I_t values again reveals a factor of $\sim$200 difference between the experimentally measured I_t values ranging from approximately 1.75–2.75 pA and the calculated I_t values ranging from approximately 6–13 fA.

2. Neutral mode tip identification

Out of phase. For the neutral mode image in Figs. 5(a) and 5(b), the image contrast closely resembles the actual geometric structure of the TiO_2(110) surface. Previously, and in Ref. 10, it was argued that a clean silicon tip would produce such a Z image contrast, making this the first restriction for discriminating between the possible tip candidates. The Z corrugation in Fig. 5(a) is very small, measuring only

a Tip 2: Si[001]-Ti$_3$O$_5$ O-terminated ([001]-aligned)
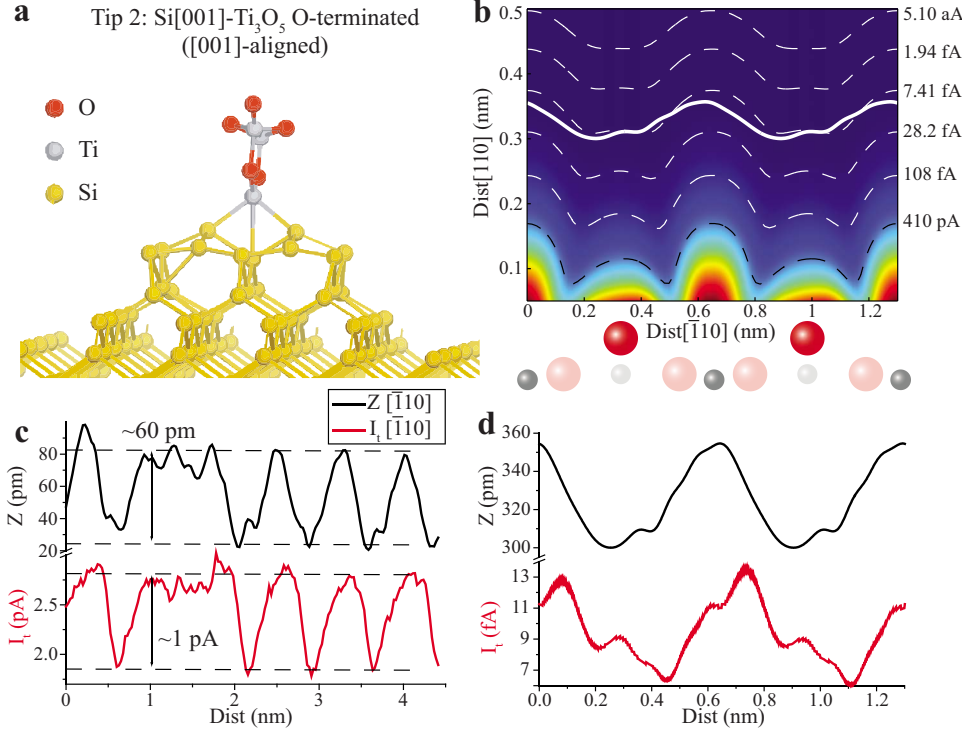
- O
- Ti
- Si

b

c

d

FIG. 10. (Color online) (a) Ball-and-stick model of Tip 2. (b) Space- and time-averaged I_t images of the full 3D calculated volume corresponding to Fig. 14(d). Six contours of constant I_t value, logarithmically and equidistantly spaced between the maximum and minimum I_t value, are shown (five white dashed and one black dashed). Inserted (solid white) is the PFF trace of the experimental Z cross section in (c) (for ball-model color code, see Fig. 8). (c) The equivalent experimental cross section from Fig. 4(c). (d) The PFF trace along with the extracted corresponding I_t values from (b).

$\sim$30 pm [see Fig. 5(d)]. This finding indicates that we should look for a silicon-terminated tip model that has the Ti(5c) rows as PTS since the contrast over the Ti(5c) rows in the I_t image in Fig. 5(c) is very pronounced and is unlikely to be caused primarily by the Z motion of the tip. However, both of the clean Si tip models, tips 3 and 4 shown in Figs. 14(e) and 14(f), have the O(2c) rows as the PTS. Upon closer inspection and a detailed comparison of the Z and I_t images in Figs. 5(a) and 5(b), it seems that the I_t image not only

contains signatures of the sOH being imaged as dark holes in between the bright rows (dashed white circles)—out-of-phase imaging—but also, signatures of the sOH being imaged on top of the bright rows (dashed white rectangles)—in-phase imaging. We use this additional observation to propose tip 3, the Si-dimer tip also shown in Fig. 11(a), as the primary tip candidate. Tip 3 has the Si-Si-dimer bond oriented perpendicular to the O(2c) and Ti(5c) rows, acting as a "double tip" for the I_t channel across the relative rough

a Tip 3: Si[001] dimer terminated ([$\bar{1}$10]-aligned)
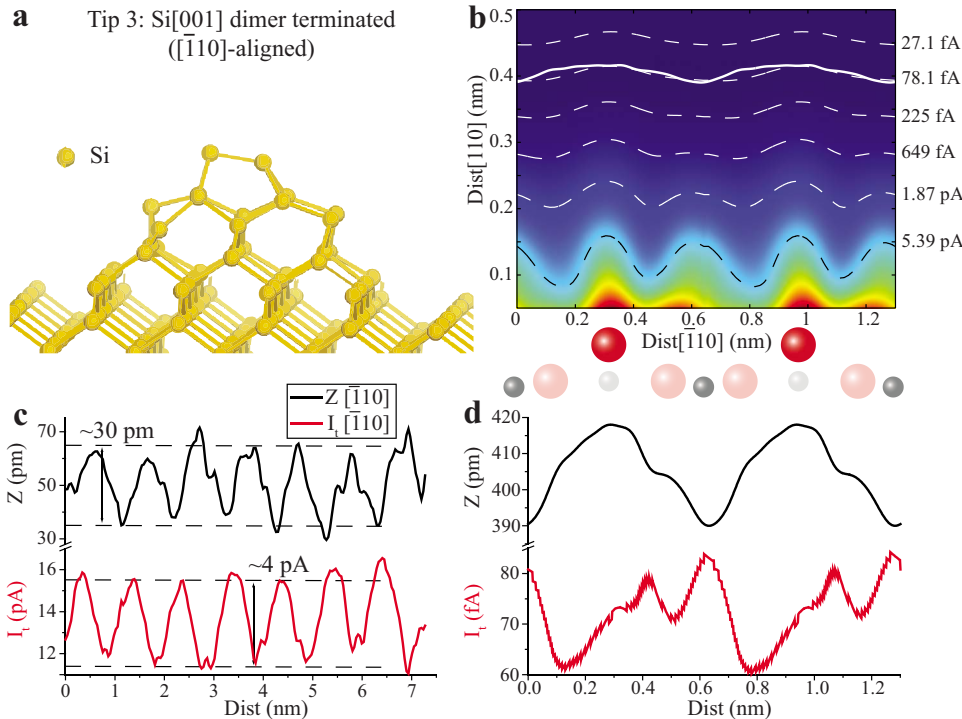
- Si

b

c

d

FIG. 11. (Color online) (a) Ball-and-stick model of tip 3. (b) Space- and time-averaged I_t images of the full 3D calculated volume corresponding to Fig. 14(e). Six contours of constant I_t value, logarithmically and equidistantly spaced between the maximum and minimum I_t value, are shown (five white dashed and one black dashed). Inserted (solid white) is the PFF trace of the experimental Z cross section in (c) (for ball-model color code, see Fig. 8). (c) The equivalent experimental cross section from Fig. 5(d). (d) The PFF trace along with the extracted corresponding I_t values from (b).
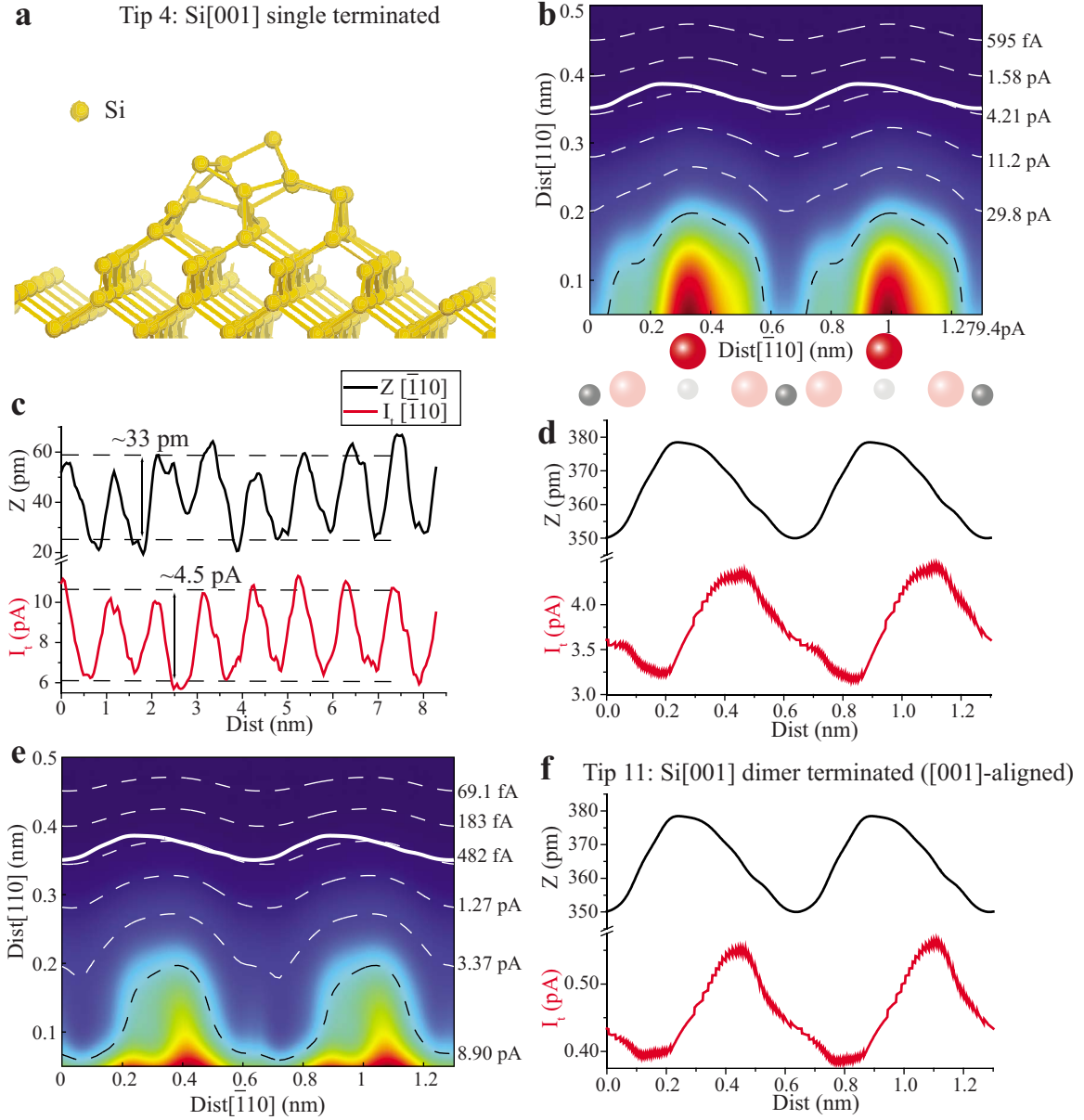
FIG. 12. (Color online) (a) Ball-and-stick model of tip 4. (b) Space- and time-averaged I_t images of the full 3D calculated volume corresponding to Fig. 14(f). Six contours of constant I_t value, logarithmically and equidistantly spaced between the maximum and minimum I_t value, are shown (five white dashed and one black dashed). Inserted (solid white) is the PFF trace of the experimental Z cross section in (c) (for ball-model color code, see Fig. 8). (c) The equivalent experimental cross section from Fig. 5(d). (d) The PFF trace along with the extracted corresponding I_t values from (b). [(e) and (f)] Equivalent to (b) and (d) only for the rotated Si-dimer tip.

TiO$_2$(110) surface. The double-tip signature is clearly visible in the calculated I_t images for the Si-dimer tip in Fig. 14(e) with a small shoulder appearing next to the dominating corrugation and even more pronounced in the averaged I_t image in Fig. 11(b), where the constant I_t contours reveal a clear double-tip signature. As the tip approaches the Ti(5c) rows, as controlled by the nc-AFM constant frequency shift feedback loop, the Si-dimer tip structure may pick up an increased I_t signal from the neighboring O(2c) row (and additionally, of sOH if one resides at this specific site), thereby generating a mixed in-phase/out-of-phase type image contrast. This analysis matches the mixed in phase/out of phase of the images in Figs. 5(a) and 5(b), making the Si-dimer tip

highly probable as a model for the tip used to record these images. The PFF fitted Z and corresponding extracted I_t curves shown in Fig. 11(d) is in qualitative very good agreement with the experimental Z and I_t cross sections in Fig. 11(c). The extracted I_t signal has a dual-peak structure with the dominating peak located exactly out of phase with respect to the Z curve, resembling the experimental data nicely. To some degree the additional smaller peak in the extracted I_t curve is also reproduced in the experimentally recorded I_t signal, where additional, although significantly smaller, peaks appear in between the primary corrugation. The extracted I_t curve in Fig. 11(d) ranges from approximately 60–80 fA, which again is the factor of ~200 less than the

a Tip 8: Si[001]-Ti$_3$O$_6$ Ti-terminated ([$\bar{1}$12]-aligned)
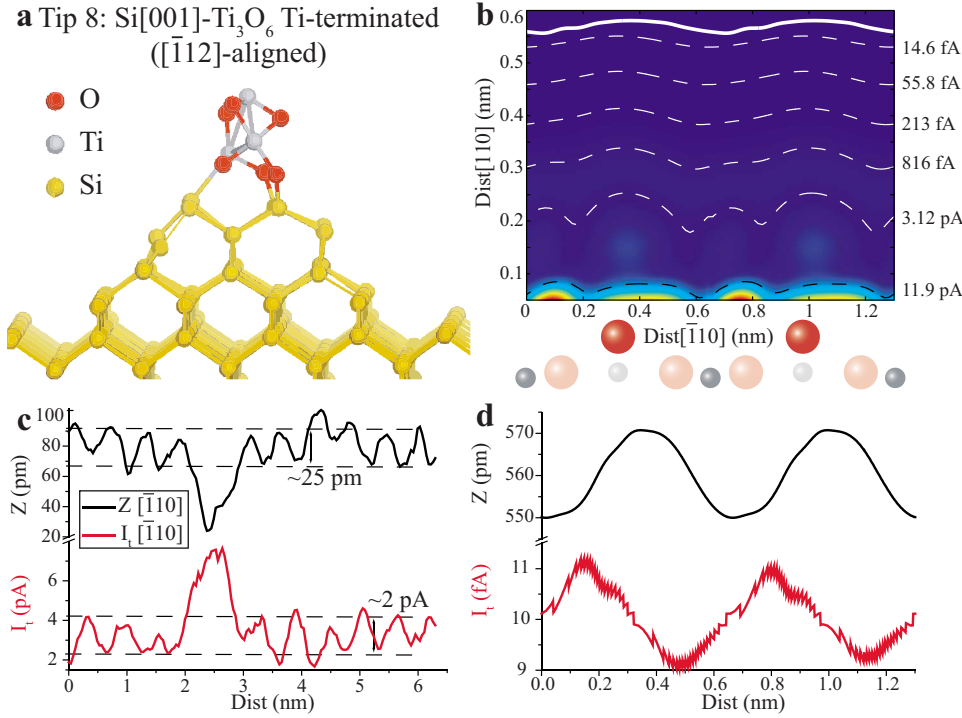
- O
- Ti
- Si

FIG. 13. (Color online) (a) Ball-and-stick model of tip 8. (b) Space- and time-averaged I_t images of the full 3D calculated volume corresponding to Fig. 15(d). Six contours of constant I_t value, logarithmically and equidistantly spaced between the maximum and minimum I_t value, are shown (five white dashed and one black dashed). Inserted (solid white) is the PFF trace of the experimental Z cross section in (c) (for ball-model color code, see Fig. 8). (c) The equivalent experimental cross section from Fig. 7(c). (d) The PFF trace along with the extracted corresponding I_t values from (b).

experimental values ranging from approximately 12–16 pA. The fact that the double-tip nature of the Si-dimer tip only shows up in the experimental I_t image and not in the Z image suggests that the covalent bonding, which is believed to be responsible for the atomic-scale contrast of Si tip images of the TiO$_2$(110) surface, is much more short ranged than the tunneling current.

In phase. For the images in Figs. 6(a) and 6(b), the in-phase imaging requires the O(2c) rows to be the PTS, matching both Si tip models. The Si single terminated tip (tip 4) now seems to be the obvious choice due to the lack of the double-tip signature, as discussed above, both in experimental line scans and in the simulations. However, the Si single terminated tip produces a factor of ~20 larger calculated I_t values, compared with the Si-dimer tip. This result disagrees with experiments as the I_t values recorded for both of the neutral mode I_t images [Figs. 5(d) and 6(d)] are very similar. The direct comparison between the calculated averaged I_t image for tip 4 and the experimentally measured I_t values from Fig. 6(b) is shown in Figs. 12(a)–12(d). A somewhat reasonable qualitative agreement is obtained with the PFF tip trace and the extracted calculated I_t curve being almost in phase [Fig. 12(d)], matching to some extent the in-phase nature of the experimentally recorded cross sections [Fig. 12(c)]. However, whereas the direct comparisons of the previous tips and images, including the comparison between the W tip and STM experiments, have revealed a consistent difference of a factor of ~200, the extracted I_t values for the Si single terminated tip ranging from approximately 3–4 pA are very close to matching the experimentally measured I_t values ranging from 6–10 pA. Since we know that the theoretical model used should underestimate the I_t calculations and the fact that all other direct comparisons presented here have revealed the same constant factor of ~200 difference, the Si single terminated tip is discarded. Since the magnitude of the

calculated I_t values for the Si-dimer tip (Fig. 11) matched the general trend of a factor of ~200 difference between calculations and experiments nicely, an additional set of I_t values was calculated using the Si-dimer tip. To remove the double-tip signature of the Si-dimer tip, it was rotated by 90°, aligning Si-Si dimer bond parallel to the O(2c) and Ti(5c) rows. In Figs. 12(e) and 12(f), the calculated averaged I_t map of the rotated Si-dimer tip and the corresponding extracted I_t curve are presented, respectively. The calculated I_t values for the rotated Si-dimer tip are, however, still roughly a factor of ~10 from matching the general factor of ~200 difference. The reason that the rotated Si-dimer tip produces a factor of ~10 larger I_t values compared with the unrotated Si-dimer tip could be that both of the terminating Si atoms participate in the tunneling process to a much larger extent on the corrugated TiO$_2$(110) surface. It is therefore tentatively proposed that a Si-dimer tip at some intermediate rotation will be able to reproduce both the experimentally recorded neutral mode in-phase images in Fig. 6(b) and match the general trend of a factor of ~200 difference in the I_t values. Unfortunately, the BSKAN code used for the calculation does not allow for arbitrary rotations of the tip with respect to the surface, and as such, it is not possible to confirm (or discard) this hypothesis at the moment.

3. Hole mode tip identification

The images in Figs. 7(a) and 7(b) were recorded in the nc-AFM hole mode, requiring a positively terminated tip to account for the bright O(2c) rows, and dark sOH and dOH groups in the Z image (see Ref. 11). From the I_t signal it is clear that the Ti(5c) rows should be the PTS, or alternatively, very weakly dominating O(2c) rows so that the Z corrugation may still govern the I_t image contrast. From these restrictions, tips 8 and 9 shown in Figs. 15(d) and 15(e) are possible choices. It is noted that tips 6 and 10 [Figs. 15(b) and
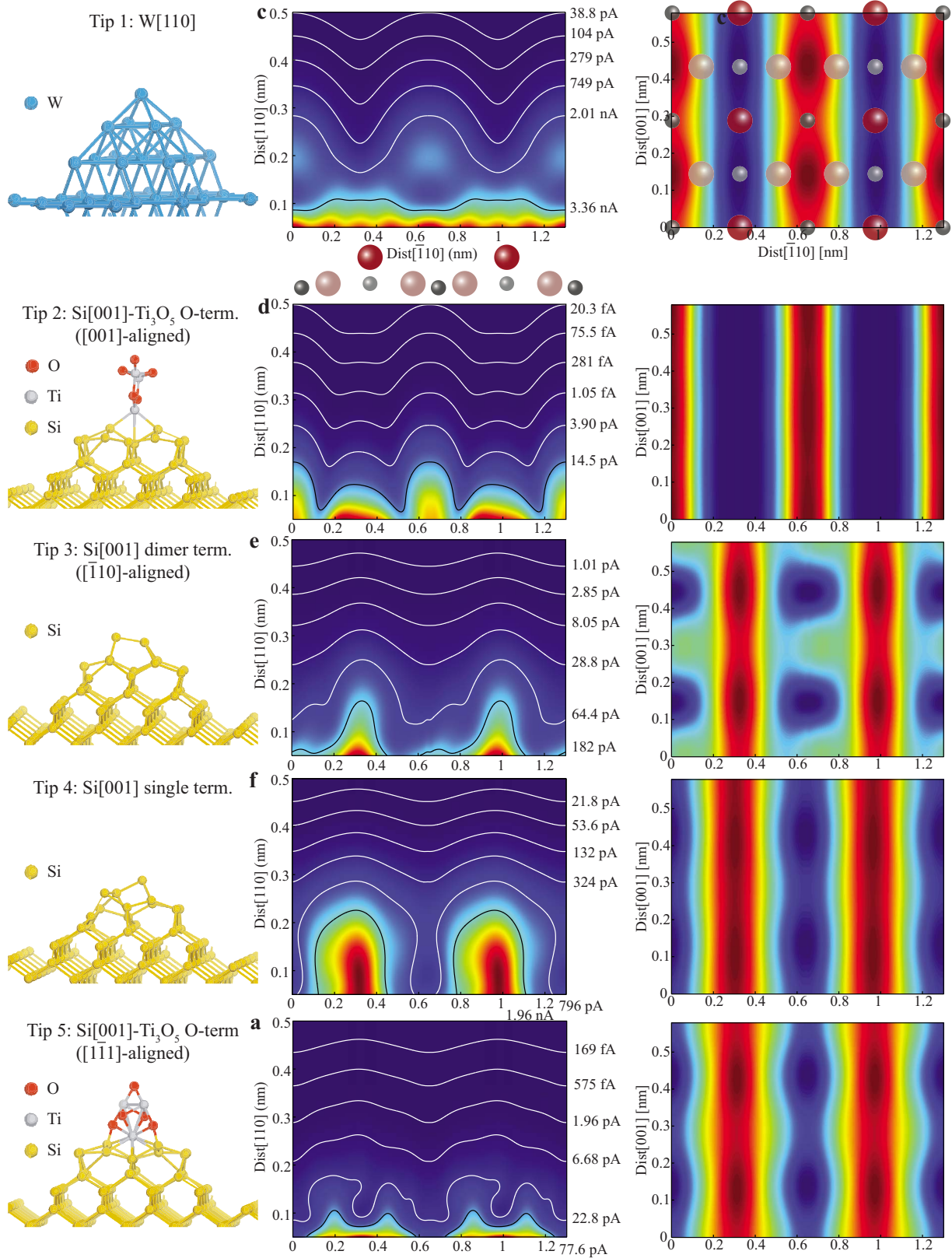
FIG. 14. (Color online) See text for details.

15(f)] are in principle also positively terminated since the OH group terminating these tips is most likely highly polarized. However, we have previously tested the nc-AFM topographic contrast generated by OH terminated tips and we found it to be far too weak to account for the Z images shown in Fig. 7(a).[11] Tips 8 and 9 are both Si-based tips terminated with a Ti_3O_6 and Ti_3O_5 nanocluster, respectively, rotated to form a Ti terminated tip apex, providing the re-
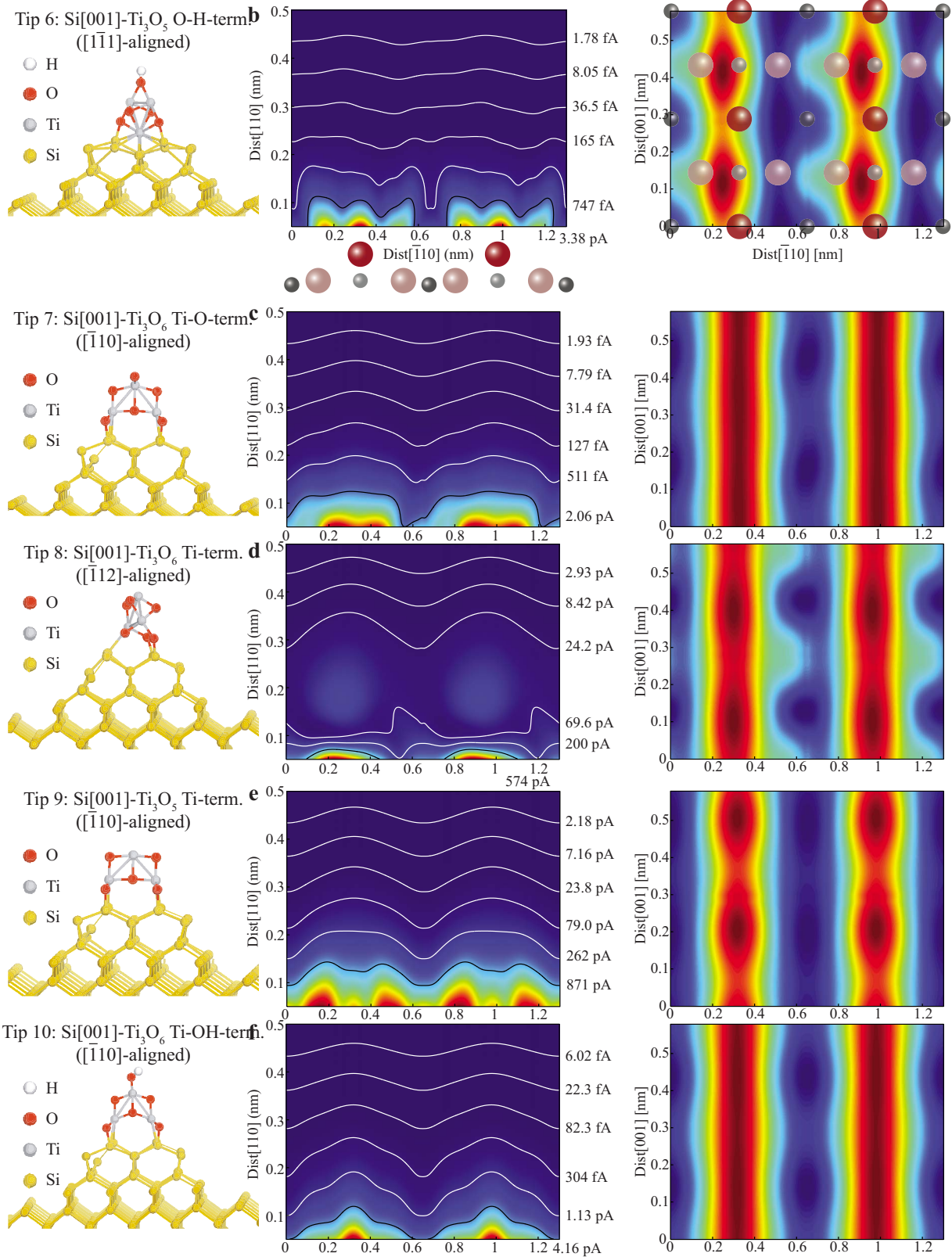
FIG. 15. (Color online) See text for details.

quired positive tip termination. According to our previous detailed analysis presented in Ref. 10, the type of *Z* image contrast in Fig. 7(a), where the sOH and dOH are clearly visible, and the corrugation between the Ti(5c) and O(2c)

rows is fairly small, is associated with relatively large imaging distances where the calculated I_t values are slightly larger for tip 8 compared to tip 9. This finding leads us to propose tip 8 as the primary tip candidate. The direct comparison

between the experimental data from Fig. 7 and the theoretically calculated I_t values for tip 8 is shown in Fig. 13, revealing a fairly good qualitative agreement. The PFF tip trace and the extracted I_t values [Fig. 13(d)] match quite well the out-of-phase signature of the experimental data [Fig. 13(b)]. A quantitative comparison reveals again the same persisting factor of ~200 between the extracted I_t values for tip 8 and the experimentally measured I_t with the experimental I_t values ranging from approximately 2–4 pA and the corresponding extracted calculated I_t values ranging from approximately 9–12 fA.

IV. CONCLUSIONS

From an interplay between experimental SPM results and theoretical calculations, we demonstrate a new method to obtain realistic atomistic models of experimental SPM tips that were used to image a $TiO_2(110)$ surface. The method relies on an expanded application of normal topographic nc-AFM imaging where the tunneling current (I_t) between the AFM tip and surface is recorded simultaneously as an additional passive signal. The complementary information thus obtained in the topographic and tunneling current channels reveal that the nc-AFM image contrast and tunneling is strongly influenced by the chemical nature of the tip apex and/or the detailed nanoscale atomic structure of the tip. We also observe a large number of different contrast combinations with no apparent correlation between the two. To determine the detailed tip-apex model for each of the observations, we first make use of the fact that the polarity of the tip apex may be determined directly from the contrast observed in the nc-AFM images. Based on this insight about the tip apex, we then build a library of chemically and structurally different atomistic tip models expected to arise when scanning a $TiO_2(110)$ surface using a silicon AFM probe. Finally, the tip termination matching the experimentally observed contours is accurately determined by simulating the nc-AFM and I_t contrast on the $TiO_2(110)$ surface for each model tip.

The present findings have several important implications. First, an accurate atomistic model of an SPM tip has in general been considered to be unachievable since a large number of possibilities involved in matching SPM tip exists and no direct information on the actual experimental tip termination is generally available. The method revealed here involving dual-channel nc-AFM/tunnel current imaging limits the number of relevant tip models considerably and, by means of this method, it is possible to generate more exact tip models than previously possible. This new method opens up for new possibilities to extract very precise quantitative and qualitative information from SPM experiments. From an interplay between experiment and theory, it is possible to enable direct chemical identification of surface species. Second, the methods revealed in this study are generally applicable and may be used for other model systems. The $TiO_2(110)$ system used in this study may thus provide a good general reference for characterization of the tip apex prior to imaging an unknown

sample. It should therefore be generally possible to identify the character of a silicon SPM probe by comparison to the presented imaging modes, and thus in principle, select a tip apex with a specific functionality for imaging of other surfaces and surface species thereon. In practice, the method to determine tip functionalization may be limited to vacuum conditions due to tip changes induced by adsorption. However, the method may become very useful by identifying and selecting a probe with a specific stability (e.g., symmetric with a high coordination of tip atoms), and by developing more reliable ways for soft approach of the AFM cantilever for imaging on other systems.

Interestingly, and perhaps surprisingly, in eight out of ten tips the calculated I_t images for the $TiO_2(110)$ surface have the O(2c) rows as PTS (see Table II). This finding stands in contradiction to results from the widely used TH approach, which predicts the Ti(5c) sites as the PTS and not the geometrically protruding O(2c) sites. Since a single adsorbate on the tip may completely change the observed contrast, these results emphasize the need for caution when interpreting STM images using TH. Finally, it is also emphasized that the ability to record the I_t simultaneously during nc-AFM imaging provides a significant increase in the accessible surface physics and chemistry offered by an SPM experiment, and can also greatly aid in distinguishing the different surface species. This finding was demonstrated by the fact that it was rather easy to separate single and double hydroxyls in the recorded I_t image while they appeared almost identical in the nc-AFM topographic image.

APPENDIX

Figures 14 and 15 depict ball-and-stick tip models (left), and corresponding direct cut (middle) and top-down constant height at $Z=0.4$ nm (right) images of the calculated tunneling current (I_t) data for all ten tips in the tip library (see Sec. II for details). The direct cut and constant height images are made from two and four identical unit-cell calculations attached to each other, respectively. The positions of the atoms are indicated by the ball model on top and below the topmost images in Figs. 14 and 15. For the direct cut images, six contours of constant I_t value, logarithmically and equidistantly spaced between the maximum and minimum I_t value for the individual I_t image, are superimposed (five white and one black), with the corresponding constant I_t value. The zero point for the [110] axis is the relaxed position of the O(2c) atoms and all direct cut images show only the [110] range from 0.05–0.5 nm for better color scaling.

[1] R. Garcia and R. Perez, Surf. Sci. Rep. **47**, 197 (2002).

[2] F. J. Giessibl, Rev. Mod. Phys. **75**, 949 (2003).

[3] W. A. Hofer, A. S. Foster, and A. L. Shluger, Rev. Mod. Phys. **75**, 1287 (2003).

[4] C. J. Chen, *Introduction to Scanning Tunneling Microscopy* (Oxford University Press, Oxford, NY, 1993).

[5] C. J. Chen, J. Phys.: Condens. Matter **3**, 1227 (1991).

[6] W. A. Hofer and A. J. Fisher, Phys. Rev. Lett. **91**, 036803 (2003).

[7] C. Loppacher, M. Bammerlin, M. Guggisberg, S. Schär, R. Bennewitz, A. Baratoff, E. Meyer, and H. J. Güntherodt, Phys. Rev. B **62**, 16944 (2000).

[8] S. Hembacher, F. J. Giessibl, J. Mannhart, and C. F. Quate, Proc. Natl. Acad. Sci. U.S.A. **100**, 12539 (2003).

[9] H. Ö. Özer, S. J. O'Brien, and J. B. Pethica, Appl. Phys. Lett. **90**, 133110 (2007).

[10] G. H. Enevoldsen, A. S. Foster, M. C. Christensen, J. V. Lauritsen, and F. Besenbacher, Phys. Rev. B **76**, 205415 (2007).

[11] J. V. Lauritsen, A. S. Foster, G. H. Olesen, M. C. Christensen, A. Kühnle, S. Helveg, J. R. Rostrup-Nielsen, B. S. Clausen, M. Reichling, and F. Besenbacher, Nanotechnology **17**, 3436 (2006).

[12] J. Tersoff and D. R. Hamann, Phys. Rev. Lett. **50**, 1998 (1983).

[13] J. Tersoff and D. R. Hamann, Phys. Rev. B **31**, 805 (1985).

[14] U. Diebold, Surf. Sci. Rep. **48**, 53 (2003).

[15] M. Guggisberg, M. Bammerlin, C. Loppacher, O. Pfeiffer, A. Abdurixit, V. Barwich, R. Bennewitz, A. Baratoff, E. Meyer, and H. J. Güntherodt, Phys. Rev. B **61**, 11151 (2000).

[16] G. Kresse and J. Furthmuller, Phys. Rev. B **54**, 11169 (1996).

[17] G. Kresse and J. Furthmuller, Comput. Mater. Sci. **6**, 15 (1996).

[18] J. P. Perdew, K. Burke, and M. Ernzerhof, Phys. Rev. Lett. **77**, 3865 (1996).

[19] G. Kresse and D. Joubert, Phys. Rev. B **59**, 1758 (1999).

[20] S. J. Thompson and S. P. Lewis, Phys. Rev. B **73**, 073403 (2006).

[21] G. Teobaldi, W. A. Hofer, O. Bikondoa, C. L. Pang, G. Cabailh, and G. Thornton, Chem. Phys. Lett. **437**, 73 (2007).

[22] R. Lindsay, A. Wander, A. Ernst, B. Montanari, G. Thornton, and N. M. Harrison, Phys. Rev. Lett. **94**, 246102 (2005).

[23] G. A. D. Briggs and A. J. Fisher, Surf. Sci. Rep. **33**, 1 (1999).

[24] K. Palotas and W. A. Hofer, J. Phys.: Condens. Matter **17**, 2705 (2005).

[25] W. A. Hofer, Prog. Surf. Sci. **71**, 147 (2003).

[26] M. Büttiker, Y. Imry, R. Landauer, and S. Pinhas, Phys. Rev. B **31**, 6207 (1985).

[27] J. A. Stroscio, D. T. Pierce, A. Davies, R. J. Celotta, and M. Weinert, Phys. Rev. Lett. **75**, 2960 (1995).

[28] S. Suzuki, K. I. Fukui, H. Onishi, and Y. Iwasawa, Phys. Rev. Lett. **84**, 2156 (2000).

[29] R. Schaub, P. Thostrup, N. Lopez, E. Laegsgaard, I. Stensgaard, J. K. Nørskov, and F. Besenbacher, Phys. Rev. Lett. **87**, 266104 (2001).

[30] U. Diebold, J. F. Anderson, K. O. Ng, and D. Vanderbilt, Phys. Rev. Lett. **77**, 1322 (1996).

[31] S. Wendt, R. Schaub, J. Matthiesen, E. K. Vestergaard, E. Wahlström, M. D. Rasmussen, P. Thostrup, L. M. Molina, E. Laegsgaard, I. Stensgaard, B. Hammer, and F. Besenbacher, Surf. Sci. **598**, 226 (2005).

[32] O. Bikondoa, C. L. Pang, R. Ithnin, C. A. Muryn, H. Onishi, and G. Thornton, Nat. Mater. **5**, 189 (2006).

[33] Z. Zhang, O. Bondarchuk, B. D. Kay, J. M. White, and Z. Dohnalek, J. Phys. Chem. B **110**, 21840 (2006).

[34] R. E. Tanner, M. R. Castell, and G. A. D. Briggs, Surf. Sci. **412-413**, 672 (1998).

[35] W. A. Hofer and J. Redinger, Surf. Sci. **447**, 51 (2000).

[36] W. A. Hofer, A. J. Fisher, R. A. Wolkow *et al.*, Phys. Rev. Lett. **87**, 236104 (2001).

[37] M. A. Henderson, Surf. Sci. **419**, 174 (1999).

[38] J. H. Becker and W. R. Hosler, Phys. Rev. **137**, A1872 (1965).

[39] E. Yagi, R. R. Hasiguti, and M. Aono, Phys. Rev. B **54**, 7945 (1996).

[40] N. Yu and J. W. Halley, Phys. Rev. B **51**, 4768 (1995).

[41] G. H. Enevoldsen, Ph.D. thesis, University of Aarhus, 2007.

[42] M. Ternes, C. P. Lutz, C. F. Hirjibehedin, F. J. Giessibl, and A. J. Heinrich, Science **319**, 1066 (2008).